CRYSTAL GROWTH & DESIGN

Article

pubs.acs.org/crystal

Exploration of Charge-Transfer Solids Utilizing Nucleobases: Nanoarchitectures by Hydrogen-Bonds in the Ionic Assemblies of Guanine and TCNQ Derivatives

Tsuyoshi Murata,*[,†] Gunzi Saito,*[,†,‡] Kenji Nakamura,[†] Mitsuhiko Maesato,[†] Takaaki Hiramatsu,[‡] and Yukihiro Yoshida[†,‡]

[†]Division of Chemistry, Graduate School of Science, Kyoto University, Oiwake-cho, Kitashirakawa, Sakyo-ku, Kyoto 606-8502, Japan

[‡]Faculty of Agriculture, Meijo University, Shiogamaguchi 1-501, Tempaku-ku, Nagoya 468-8502, Japan

Supporting Information

ABSTRACT: We studied formation and structural characteristics of charge-transfer solids of 9-*n*-butylguanine (**BuG**) with fluorinated tetracyanoquinodimethane derivatives (F_nTCNQ, n = 4, 2, and 1). Complex formation in a methanol (MeOH)-containing solvent generated two types of salts composed of either a methoxy-substituted anion or a fully ionic anion radical of F_nTCNQ. In all anion radical salts, **BuG** existed as a protonated or a hemiprotonated species, **BuGH**$^+$ or (**BuG**)-(**BuGH**$^+$), respectively, and formed hydrogen-bonded (H-bonded) assemblies. In these **BuGH**$^+$ assemblies, $F_nTCNQ^{\bullet-}$ molecules were fixed and aligned periodically, providing H-bonded polycationic templates. In (**BuGH**$^+$)($F_4TCNQ^{\bullet-}$), **BuGH**$^+$ dimers by complementary H-bonds formed a two-dimensional (2D) polycationic sheet. The $F_4TCNQ^{\bullet-}$ face-to-face dimers formed a one-dimensional (1D) segregated column aided by formation of H-bonds with **BuGH**$^+$. In (**BuGH**$^+$)-($F_2TCNQ^{\bullet-}$)(MeOH), **BuGH**$^+$ dimers by complementary double H-bonds formed a 1D polycationic ribbon supported by MeOH-mediated H-bonds. A 1D mixed stack column of (**BuGH**$^+$)$_2$ and ($F_2TCNQ^{\bullet-}$)$_2$ dimers was formed owing to their complementary geometry and size. In (**BuG**)(**BuGH**$^+$)($F_1TCNQ^{\bullet-}$), a new type of **BuG**−**BuGH**$^+$ pair formed a 1D ribbon supported by complementary H-bonds, and $F_1TCNQ^{\bullet-}$ dimers were aligned by H-bonds with the **BuG**−**BuGH**$^+$ ribbon.

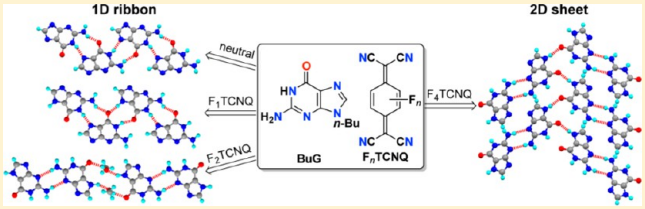

INTRODUCTION

One-dimensional (1D) π-stacks of nucleobases are regarded as the hole transport path of DNA, and many exciting, controversial transport properties of DNA, such as metallic or proximity superconducting electrical conduction, have been reported in recent studies of biomolecule-based materials.[1−4] Formation of such a path in DNA is one example of a biosupramolecular architecture based on the self-assembling ability of nucleobases by complementary hydrogen-bonds (H-bonds).[5] For the development of organic conductors, such highly selective, directional, and robust H-bonds have been utilized as an effective tool to control not only molecular arrangements with a variety of dimensionality in real space[6] but also the electronic dimensionality and structures in k-space.[7] Nucleobases have been utilized to control molecular arrangements in organic conductors, and tetrathiafulvalene (TTF, Scheme 1) derivatives having nucleobase skeletons[8,9] have been designed and synthesized. These donor molecules form diverse supramolecular assemblies based on the complementary H-bonds of nucleobases and have provided several conductive charge-transfer (CT) solids.[8,9] Previously, we investigated CT solids prepared by mixing cytosine (**C**, Scheme 1) in methanol (MeOH) and tetracyanoquinodimethane derivatives (RTCNQ, Scheme 1) in acetonitrile (MeCN)[10] and observed formation of three types of ionic solids: (**I**) insulators composed of methoxy-substituted RTCNQ anions, (**II**) semiconducting fully ionic RTCNQ radical anion salts, and (**III**) highly conductive partially ionic or mixed-valence RTCNQ radical anion salts. Also, we studied formation of CT solids between **C** species and Ni(dmit)$_2$ (Scheme 1) and obtained fully ionized insulators of Ni(dmit)$_2^{\bullet-}$, and semiconductive and metallic conductors of partially ionized Ni(dmit)$_2^{0.5-}$.[11] As for the **C** species, in all cases, **C** preferentially behaves as a proton-acceptor, but not an electron-donor, and becomes a protonated (**CH**$^+$) or a hemiprotonated (**CHC**$^+$, Scheme 1) cation whose H-bond-mediated self-assembling ability enables construction of uniform supramolecular frameworks. Furthermore, the H-bonds between the **C** species and RTCNQ afforded a robust 3D architecture, in which a Mott insulator (**CHC**$^+$)($TCNQ^{\bullet-}$) retained its uniform 1D framework down to 10 K despite the fact that a typical 1D electronic lattice is very susceptible to lattice distortion (spin-Peierls transition).[10,12] Nucleobases possess multiple H-bonding sites forming further diverse self-assembled architectures.[5] These foregoing studies suggest the high potential of self-assembling ability of nucleobases as structural templates for anion radical molecules, and further

Received: January 11, 2013
Revised: May 19, 2013
Published: May 30, 2013

Scheme 1. Molecular Structures of Guanine (G), Cytosine (C), Hemiprotonated Cytosine (CHC^+), RTCNQ, TTF, and $Ni(dmit)_2$[a]

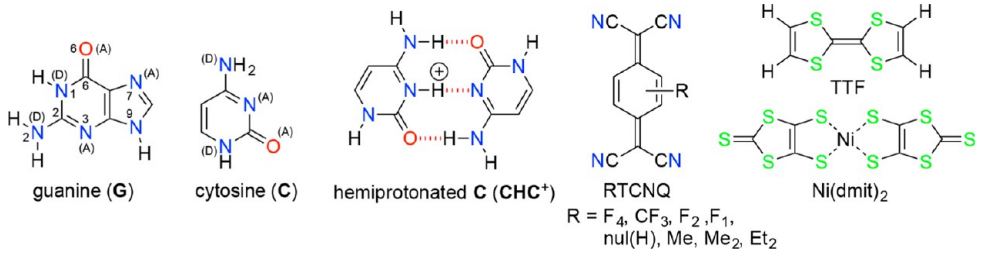

[a](D) and (A) in **G** and **C** indicate the H-bond donating and accepting sites, respectively.

Scheme 2. H-Bonded 1D Ribbons Observed in Neutral G Derivatives (Ribbon-A (a) and Ribbon-B (b)),[17] (CHC^+)($TCNQ^{\bullet-}$) (c),[10a] and (CHC^+)(2,5-diethyl-$TCNQ^{\bullet-}$) (d),[10a,b] Complementary Triple H-Bonds in Partially Deprotonated Guanine (Left)[21a] and Hemiprotonated 7,9-Dimethylguanine Pairs (Right) (e),[21b] and H-Bonded 1D Ribbon of Hemiprotonated Guanine Pairs (f)[21d,e] [a]

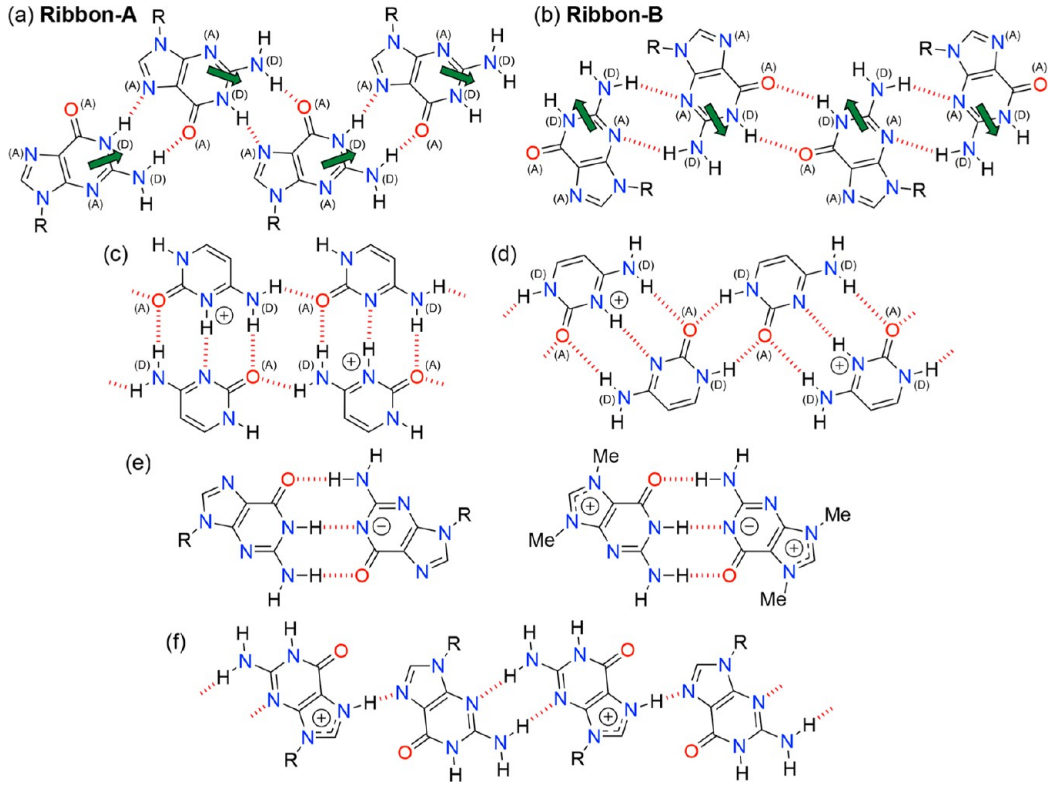

[a]Green arrows in a and b indicate the dipole. D and A in a–d indicate the H-bond donating and accepting sites, respectively.

investigations of CT solids of nucleobases are essential for the development of organic conductors.

Guanine (**G**, Scheme 1) is a stronger electron-donor (E_{ox} = +1.25 V vs SCE;[13] ionization potential I_p = 7.77–7.85 eV[14]) than **C** (+1.90 V,[13] 8.45–8.68 eV[14]), but still much weaker than TTF (+0.34 V, 6.4 eV[15]). The nucleobase **G** has three H-bond accepting sites (N7, N3, and O6; denoted as A in Scheme 1) and two H-bond donating sites (N1 amide and N2 amino group, denoted as D in Scheme 1), while **C** has two H-bond donating and two accepting sites. Similar to **C**, **G** is a Brønsted acid and a base (pK_a = 3.3, 9.2, and 12.3 vs 4.45 and 12.2 for **C**),[16] and readily forms a protonated cation (GH^+).

Neutral **G** forms various supramolecular H-bonded structures, such as dimers, **G**-quartets, **G**-quadruples, and 1D ribbons.[17] In the 1D ribbons of neutral **G** derivatives, two H-bonding patterns with different H-bond donating and accepting sites have been reported (Ribbon-A and Ribbon-B in Schemes 2a and 2b, respectively). In Ribbon-A, a **G**–**G** pair is formed with two H-bond donating sites on one **G** (N1 amide and N2 amino) and two H-bond accepting sites on the other **G** (O6 and N7), and the net dipole is retained. On the other hand, in Ribbon-B, **G**–**G** pairs are formed with double N1–H···O6 and N2–H···N3 H-bonds in each **G** unit, resulting in quenching of the net dipole.

Similar H-bonded 1D ribbon motifs have been observed in assemblies of neutral **C**[18] and its derivatives[19] as well as CH^+ and CHC^+.[10,11,20] Furthermore, multiple H-bond connections between neighboring ribbons modulate the relative positioning of **C**, CH^+, and CHC^+ molecules to provide 1D H-bonded ribbons, 2D H-bonded sheets, and 3D H-bonded net-

dx.doi.org/10.1021/cg400059h | Cryst. Growth Des. 2013, 13, 2778–2792

works.[10,11,17−20] Schemes 2c and 2d illustrate two types of **CHC**$^+$ 1D ribbons observed in the RTCNQ CT solids. Each **CHC**$^+$ unit is connected to each other with double N(amino)−H···O (Scheme 2c) or N(amido)−H···O (Scheme 2d) H-bonds on the same side. Similar to **CHC**$^+$, **G** derivatives form hemideprotonated **G** pairs by triple H-bonds (Scheme 2e).[21a−c] Furthermore, a 1D infinite ribbon is formed by the N7−H···N7 H-bond of a pair of **GH**$^+$ and **G** species (Scheme 2f).[21d,e]

One of the most fascinating features of utilizing **C** in the study of CT solids[10,11] is that 1D **CHC**$^+$ ribbons, shown in Schemes 2c and 2d, afford polycationic templates that have multiple periodic H-bonding sites to anion radicals, which have exhibited unprecedented crystal structures and solid-state transport and magnetic properties. Such templates are expected to be common among the protonated nucleobases, including **G** derivatives.

It is difficult to dissolve **G** in conventional organic solvents, preventing from the synthesis of CT solids with various acceptor molecules. We prepared 9-*n*-butylguanine (**BuG**, Scheme 3), in which an N^9 H-bonding site was quenched by an *n*-butyl group to improve the solubility, and studied the preparation and structural features of its CT solids with some RTCNQs. Since **BuG** served as a proton-acceptor, not as an electron-donor, to give a protonated cation, similar to **C**, we elucidated the function of **BuG** as a source of polycationic templates. A preliminary result with F_1TCNQ CT solids was reported.[22]

Scheme 3. Molecular Structures of Neutral and Protonated 9-*n*-Butylguanine (BuG and BuGH$^+$, Respectively)[a]

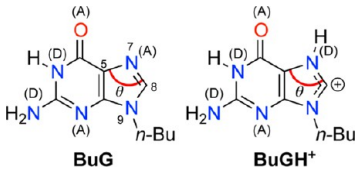

[a]C5−N7−C8 bond angle is shown by θ (°). (D) and (A) indicate the H-bond donating and accepting sites, respectively.

RESULTS AND DISCUSSION

Preparation of BuG and Its Suitability as an Electron-Donor Molecule. **BuG** was prepared from 2-amino-6-chloropurine in two steps as described in the Experimental Section. **BuG** is soluble in alcohols, *N*,*N*-dimethylformamide, dimethylsulfoxide, ethylene glycol, and pyridine, but insoluble in tetrahydrofuran, ethyl acetate, acetone, MeCN, and halogenated solvents. **BuG** is a slightly stronger electron-donor (E_{ox}^{peak} = +1.22 V vs SCE) than **G**, although its strength is not sufficient to ionize even F_4TCNQ (E_{red}^{peak} = +0.53 V vs SCE). The redox potential difference ($\Delta E(DA) = E_{ox} - E_{red}$) between **BuG** and RTCNQs does not meet the requirements for a partial CT state: $-0.02 \le \Delta E(DA) \le 0.34$ V.[23]

Crystal Structure of BuG. Table 1 summarizes the crystallographic data of **BuG**. There are three crystallographically independent **BuG** molecules (**BuG-A**−**C**, Figure 1). **BuG-A** forms a 1D infinite ribbon (denoted as the A-ribbon; width of 7.5 Å (except the *n*-butyl groups)) along the *b* axis supported by H-bonds with the same H-bonding pattern shown in Scheme 2a (Figure 2a, amino N2A−H···O═C, 2.77 Å and amide N1A−H···imino N7A, 2.81 Å; H-bonds shorter than the sum of van der Waals (vdW) radii[24] are summarized in Supporting Information Table S1). Also, a unique infinite 1D ribbon is formed by **BuG-B** and **BuG-C** (denoted as the BC-ribbon; width of 7.5 Å (except the *n*-butyl groups)), which are alternatingly arranged along the *a* axis with the same type of H-bonds as the A-ribbon (amino N2B−H···O═C, 2.88 Å; and amino N2C−H···O═C 2.89 Å; amide N1B−H···imino N7C, 2.85 Å; amide N1C−H···imino N7B, 2.79 Å, Figure 2b). The **G** skeletons in the A-ribbon are nearly parallel to each other and have a small twist angle (2.6°), while the molecular planes of

Table 1. Crystallographic Data of BuG and Charge-Transfer Solids (1 and 3)

	BuG	1, (BuGH$^+$)(F_4TCNQ$^{\bullet-}$)	3, (BuGH$^+$)(F_2TCNQ$^{\bullet-}$)(MeOH)
formula	$C_9H_{13}N_5O_1$	$C_{21}H_{14}N_9F_4O_1$	$C_{22}H_{20}N_9F_2O_2$
formula weight	207.24	484.40	480.46
crystal system	orthorhombic	monoclinic	triclinic
space group	$P2_12_12_1$	$I2/a$	$P\bar{1}$
crystal size (mm^3)	0.30 × 0.20 × 0.15	0.30 × 0.02 × 0.02	0.30 × 0.10 × 0.10
a (Å)	11.029(1)	21.835(2)	10.219(4)
b (Å)	10.759(2)	6.8446(3)	10.475(2)
c (Å)	26.357(4)	29.771(3)	12.735(4)
α (deg)			69.56(3)
β (deg)		99.016(8)	85.46(3)
γ (deg)			61.98(3)
V (Å^3)	3127.5(8)	4394.4(6)	1121.7(9)
Z	12	8	2
D_{calcd} (g cm^{-3})	1.320	1.464	1.423
temperature (K)	200	290	290
μ (cm^{-1})	0.093[c]	1.047[d]	0.109[c]
no. of reflections measured	3507	19751	5452
no. of independent reflections	3507	4016	5168
no. of reflections used	2484	2381	2185
no. of refined parameters	406	316	376
R_1 ($I > 2\sigma(I)$)[a]	0.115	0.0613	0.0704
R_2 (all data)[b]	0.333	0.1935	0.2219
GOF	1.329	1.050	0.998

[a]$R_1 = \Sigma(|F_0| - |F_c|)/\Sigma|F_0|$. [b]$R_2 = [\Sigma w(F_0^2 - F_c^2)^2/\Sigma w(F_0^2)^2]^{0.5}$. [c]Mo K$\alpha$. [d]Cu K$\alpha$.

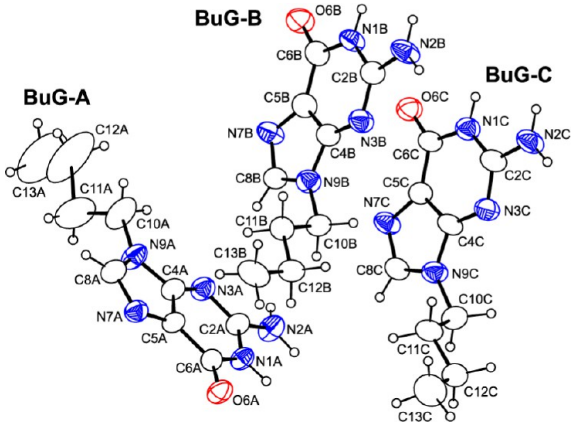

Figure 1. Molecular structures of **BuG** (A, B, and C) showing the atom labeling scheme.

dx.doi.org/10.1021/cg400059h | Cryst. Growth Des. 2013, 13, 2778−2792

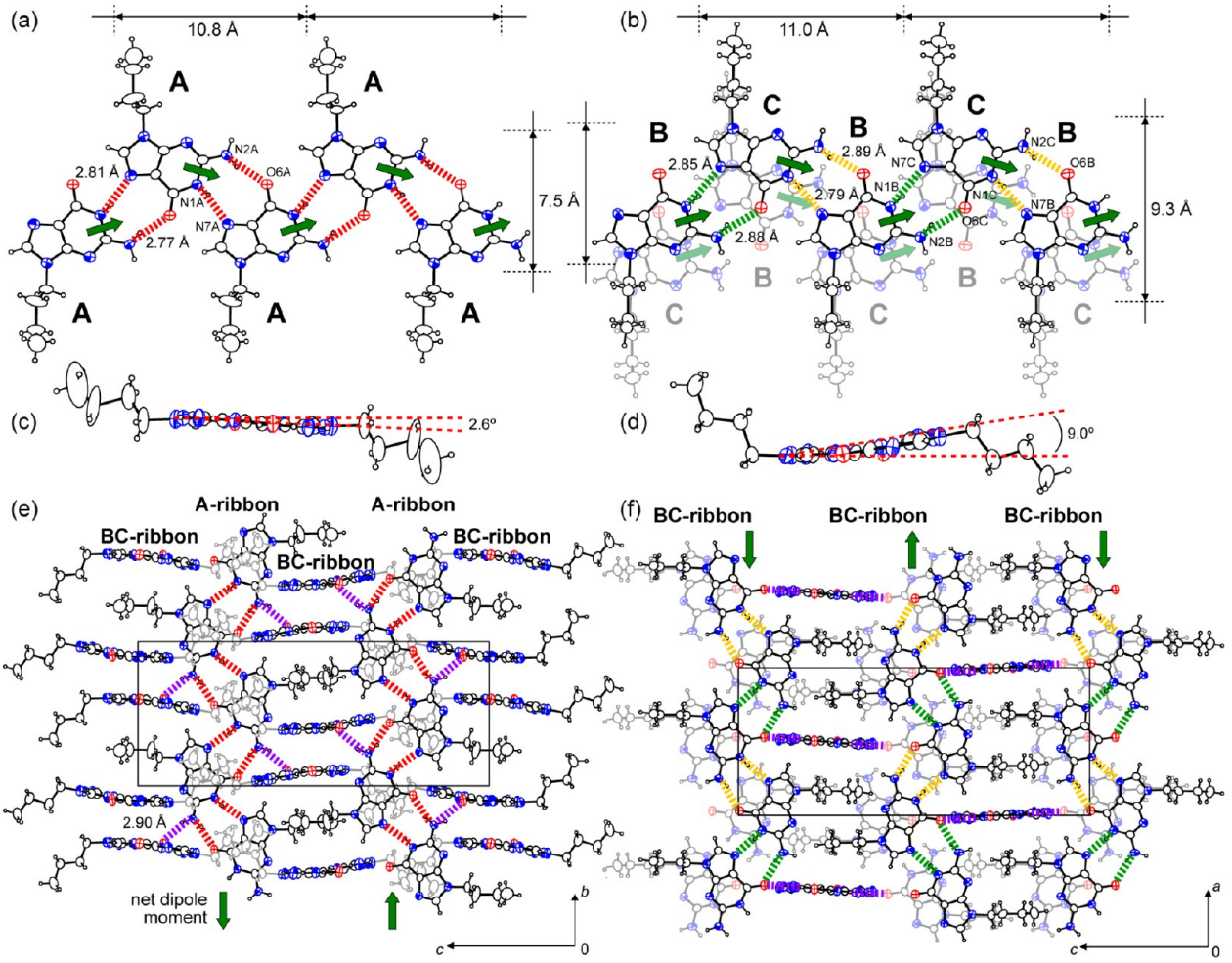

Figure 2. Crystal structure of neutral **BuG**. H-bonded infinite 1D ribbons composed of molecule A (a) and molecules B and C (b). In panel b, the π-overlap of the dimerized BC-ribbons is shown by the half-colored molecules. Green arrows indicate the directions of the dipole of each molecule. (c and d) Projections of the A-ribbon (a) and BC-ribbon (b), viewed along the ribbon directions, showing the twisting angles of adjacent molecules. (e) Crystal structure viewed along the *a* axis showing two adjacent A-ribbons and the interactions between the A- and BC-ribbons. (f) Crystal structure viewed along the *b* axis showing three neighboring dimerized BC-ribbons and interactions between the A- and BC-ribbons. H-bonds within the A-ribbon and BC-ribbon, and those between the A- and BC-ribbons are indicated by red, green, and orange, and purple dotted lines, respectively, with bond lengths (Å).

Table 2. H-Bonded Ribbons and Dipole Moments

Compound	Structural characteristic of ribbon	Dipole of each ribbon	Net dipole character
neutral **BuG**	A-ribbon, 1D } 3D network	Dipole alive	Adjacent ribbon runs in the opposite direction: no net dipole
	BC-ribbon, 1D } 3D network	Dipole alive	Adjacent dimerized ribbons run in the opposite direction: no net dipole
1, (**BuGH**$^+$)(F_4TCNQ$^{\bullet-}$)	2D layer	No dipole	Repeating unit of ribbon (dimer of **BuGH**$^+$) has no dipole
3, (**BuGH**$^+$)(F_2TCNQ$^{\bullet-}$)(MeOH)	MeOH-mediated ribbon, 1D	No dipole	Active repeating unit of ribbon (dimer of **BuGH**$^+$) has no dipole
5, (**BuG**)(**BuGH**$^+$)(F_1TCNQ$^{\bullet-}$)	(**BuG**)(**BuGH**$^+$) ribbon, 1D	Dipole alive	Adjacent ribbon runs in the opposite direction (both A and B-types): no net dipole

BuG-B and **BuG-C** in the BC-ribbon twist by 9.0° with respect to each other (Figures 2c and 2d).

The arrangement of dipole moments of component molecules is important to the determination of relative

dx.doi.org/10.1021/cg400059h | *Cryst. Growth Des.* 2013, 13, 2778−2792

molecular orientation, and is also essential for intriguing solid state properties such as ferroelectricity and pyroelectricity in the H-bonded crystals.[25] Table 2 summarizes the nature of the H-bonded ribbons and their dipoles observed in this study. As shown by the green arrows in Figures 2a and 2b, both the A-ribbon and BC-ribbon have substantial permanent dipoles; however, the crystal does not have a net dipole for the following reasons. Each infinite A-ribbon is aligned along the *c* axis with adjacent ribbons running in the opposite direction, canceling out the net dipole (Figure 2e). The BC-ribbon forms a π-stacked pair with a small $\pi-\pi$ overlap between **BuG-B** and **BuG-C** (Figure 2b; interplanar distance, 3.33 Å and width, 9.3 Å). It is noticeable that dipole moments of each ribbon in a pair are parallel to each other and that dimerization of the 1D infinite BC-ribbons does not lead to cancellation of the dipoles. However, the dimerized BC-ribbons are aligned along the *c* axis with adjacent dimerized ribbons running in the opposite direction, and this extended assembly does cancel out the net dipole (Figure 2f).

One of the most characteristic features of neutral **BuG** crystals is that the two types of ribbons run in perpendicular directions and are connected to each other by H-bonds (purple dotted lines, Figure 2e, 2.90 Å) between amino groups of **BuG-A** and carbonyl groups of **BuG-B** (N2A–H···O6B), constructing a H-bonded 3D network (Supporting Information Figure S1). The *n*-butyl groups of both ribbons are aligned parallel to the molecular plane to fill the 4–5 Å voids (Figures 2e and 2f).

Preparation and Classification of Products. Table 3 lists the products obtained by mixing **BuG** and F_nTCNQ (n = 4, 2, and 1) in mixed solvents with MeOH. The weaker acceptor TCNQ did not afford $TCNQ^{\bullet-}$ salts as solid products, although the solution turned blue, indicating the formation of the $TCNQ^{\bullet-}$ anion radicals.

Table 3. Appearance, Assignment, and Composition of the Reaction Products between BuG and F_nTCNQ (n = 4, 2, and 1)[a]

TCNQ	solvent	no.	appearance	group	composition
F_4TCNQ	MeOH/MeCN	**1**	dark blue rod	**II**	(**BuGH**$^+$)($F_4TCNQ^{\bullet-}$)
		2	pale green powder	**I**	mixture of F_4TCNQ-OMe$^-$ salt
F_2TCNQ	MeOH/1,2-dichloroethane	**3**	dark blue rod	**II**	(**BuGH**$^+$)($F_2TCNQ^{\bullet-}$)(MeOH)
		4	green powder	**I**	mixture of F_2TCNQ-OMe$^-$ salt
F_1TCNQ	MeOH/MeCN	**5**	blue plate	**II**	(**BuG**)(**BuGH**$^+$)($F_1TCNQ^{\bullet-}$)
		6	green powder	**I**	mixture of F_1TCNQ-OMe$^-$ salt

[a]Groups **I** and **II** salts are illustrated in Scheme 4.

Mixing a solution of BuG in MeOH with a solution of F_nTCNQ in MeCN (or 1,2-dichloroethane or benzonitrile) yielded a dark blue to green solution, indicating the generation of the $F_nTCNQ^{\bullet-}$ species. The blue crystals suitable for structural analysis (Group **II** salts, **1** for n = 4, **3** for n = 2, and **5** for n = 1, Supporting Information Figure S2) were isolated by recrystallization from a MeOH solution of the concentrated (or dried) reaction mixture. The crystals of **3** gradually loose crystal solvent (MeOH) in open air. The ratios of **BuG** to F_nTCNQ species in **1** and **5** were determined as 1:1 and 2:1, respectively, from elemental and crystal structure analyses (Table 3). For **3**, the ratio was determined by crystal structure analysis only. Evaporation of the filtrate yielded a green powder (**2** for n = 4, **4** for n = 2, and **6** for n = 1). A spectroscopic study of these compounds indicated that the major components of the filtrates were salts of the methoxy-substituted F_nTCNQ anions (F_nTCNQ-OMe$^-$, Group **I** salts), although further purification to isolate the corresponding salts was not successful (vide infra). As shown in the reaction between **C** and F_nTCNQ in MeOH and MeCN,[26] nucleophilic addition of MeOH to F_nTCNQ produces an acidic adduct, which is easily deprotonated by **BuG** to generate a salt of protonated **BuG** (**BuGH**$^+$, Scheme 3) and F_nTCNQ-OMe$^-$ (i.e., a Group **I** salt of (**BuG**)$_m$(**BuGH**$^+$)(F_nTCNQ-OMe$^-$)) (Scheme 4). One-electron transfer from F_nTCNQ-OMe$^-$ to neutral F_nTCNQ results in the formation of $F_nTCNQ^{\bullet-}$ (Scheme 4) to give the Group **II** salt (**BuG**)$_m$(**BuGH**$^+$)($F_nTCNQ^{\bullet-}$).

Spectroscopic Features. IR spectra of **1** and **2** in the C≡N stretching (Figure 3a, 2050–2300 cm^{-1}) and C=C and C=O stretching regions (Figure 3b, 1450–1800 cm^{-1}) are shown in Figure 3 and are compared with those of F_4TCNQ, $K^+F_4TCNQ^{\bullet-}$, and the **C**–F_4TCNQ ((**CHC**$^+$)($F_4TCNQ^{\bullet-}$) and (**CHC**$^+$)(F_4TCNQ-OMe$^-$)(H_2O)).[26] Salt **1** exhibits three C≡N stretching peaks in the 2180–2210 cm^{-1} region, which are ascribed to the $F_4TCNQ^{\bullet-}$ species. The peaks are shifted to lower frequencies than $K^+F_4TCNQ^{\bullet-}$ and are similar to those observed for (**CHC**$^+$)($F_4TCNQ^{\bullet-}$); the shape is more complicated than those of these two salts. The difference in the shape may originate from the difference in the stacking modes of $F_4TCNQ^{\bullet-}$ in the crystal structures (vide infra). The shape and location of the peaks for the C≡N stretching modes of **2** (2154 and 2194 cm^{-1}) are markedly different from those of $K^+F_4TCNQ^{\bullet-}$, **1**, and (**CHC**$^+$)($F_4TCNQ^{\bullet-}$); however, they are very similar to those observed for (**CHC**$^+$)(F_4TCNQ-OMe$^-$)(H_2O) (2153 and 2193 cm^{-1}), indicating formation of the F_4TCNQ-OMe$^-$ species in the reaction between **BuG** and F_4TCNQ in MeOH/MeCN (Scheme 4).

In the C=C and C=O stretching region (Figure 3b), the bands above 1620 cm^{-1} are ascribable to either **BuG** or **BuGH**$^+$; both **1** and **2** show a broad band at 1700 cm^{-1} which corresponds to **BuGH**$^+$, and no band ascribable to neutral **BuG** is detected. Salt **1** exhibits bands at 1540 and 1503 cm^{-1} corresponding to $F_4TCNQ^{\bullet-}$, while **2** exhibits a broad band around 1480–1500 cm^{-1} corresponding to F_4TCNQ-OMe$^-$.

Figure 4 compares the UV–vis-NIR spectra of **1** and **2** with those of $K^+F_4TCNQ^{\bullet-}$, (**CHC**$^+$)($F_4TCNQ^{\bullet-}$), and (**CHC**$^+$)-(F_4TCNQ-OMe$^-$)(H_2O).[26] The spectrum of **1** is very similar to that of (**CHC**$^+$)($F_4TCNQ^{\bullet-}$) and has peaks at 12 × 10^3, 15 × 10^3, and 27 × 10^3 cm^{-1}, denoted as C, D, and E bands, respectively, which are ascribable to the intramolecular transitions of $F_4TCNQ^{\bullet-}$. The broad band at 7.5 × 10^3 cm^{-1} (denoted as the B band) is originated from the intermolecular transition between $F_4TCNQ^{\bullet-}$ species. The band appears at an energy region higher than that observed for $K^+F_4TCNQ^{\bullet-}$ (6.2 × 10^3 cm^{-1}), indicating **1** has a loose 1D segregated column or a dimerized nature. Compared with the rather sharp band in $K^+F_4TCNQ^{\bullet-}$, the B band of **1** is markedly broad strongly suggesting that it consists of both intra- and interdimer transitions. The absence of any absorption bands below 5 × 10^3 cm^{-1}, which originate from the intermolecular transition in the mixed-valence state, confirms the fully ionic nature of **1**.

dx.doi.org/10.1021/cg400059h | *Cryst. Growth Des.* 2013, 13, 2778–2792

Scheme 4. Formation Mechanism of $F_nTCNQ\text{-}OMe^-$ and $F_nTCNQ^{\bullet-}$ in the Presence of BuG in MeOH

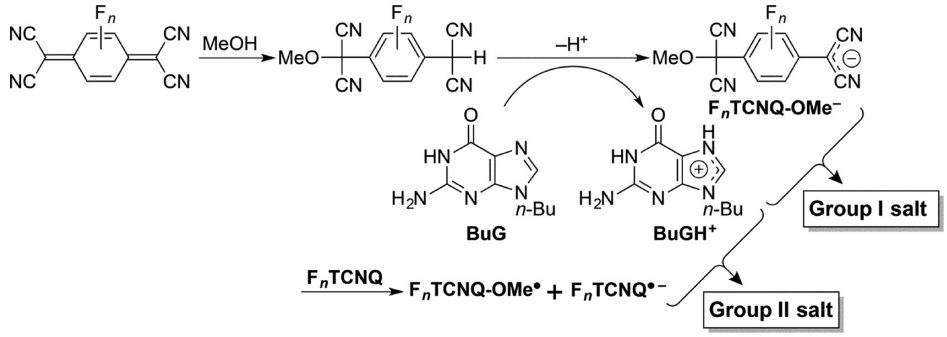

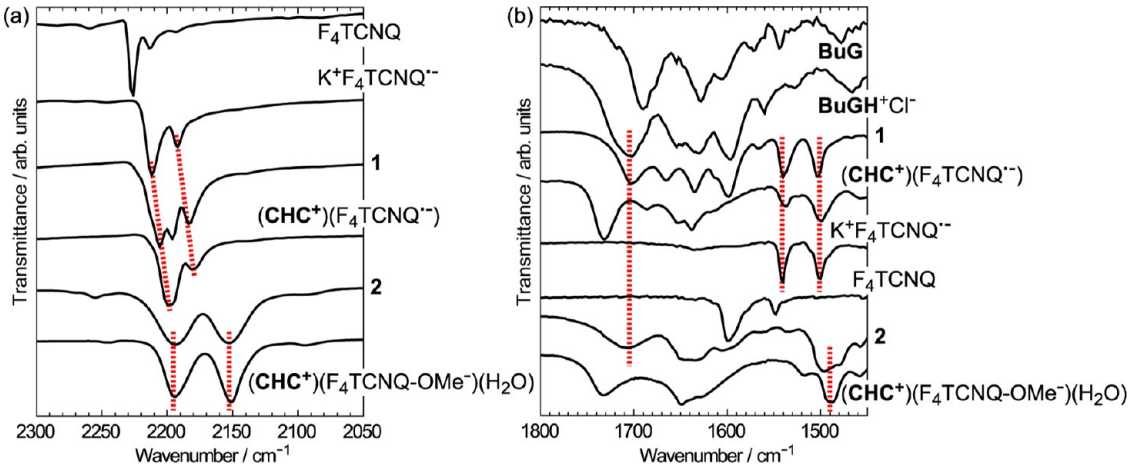

Figure 3. IR spectra of **1** and **2** together with those of F_4TCNQ, $K^+F_4TCNQ^{\bullet-}$, $(\mathbf{CHC}^+)(F_4TCNQ^{\bullet-})$, $(\mathbf{CHC}^+)(F_4TCNQ\text{-}OMe^-)(H_2O)$, **BuG**, and $\mathbf{BuGH}^+\mathbf{Cl}^-$: (a) C≡N region and (b) C═C and C═O region. Red lines are guides to eyes.

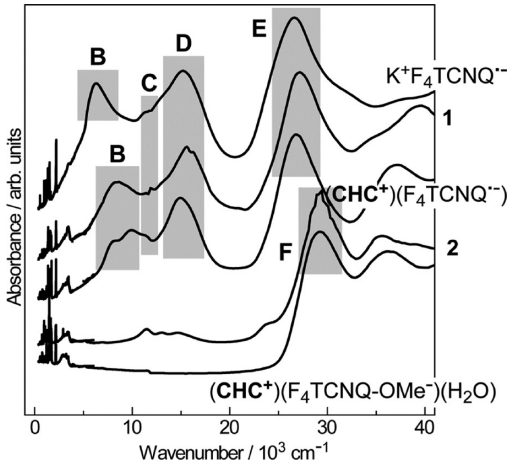

Figure 4. UV–vis-NIR spectra of **1** and **2** together with those of $K^+F_4TCNQ^{\bullet-}$, $(\mathbf{CHC}^+)(F_4TCNQ^{\bullet-})$, and $(\mathbf{CHC}^+)(F_4TCNQ\text{-}OMe^-)(H_2O)$. For bands B–F, see text.

The strong band of **2** around 29×10^3 cm^{-1} (denoted as the F band) corresponds to the intramolecular transition of $F_4TCNQ\text{-}OMe^-$ as observed for $(\mathbf{CHC}^+)(F_4TCNQ\text{-}OMe^-)(H_2O)$. Salt **2** also shows weak bands around $10–15 \times 10^3$ cm^{-1} that are ascribable to $F_4TCNQ^{\bullet-}$ species. This fact suggests that **2** is mainly composed of $F_4TCNQ\text{-}OMe^-$ species but contaminated with a small amount of $F_4TCNQ^{\bullet-}$ species. A pure $F_4TCNQ\text{-}OMe^-$ salt should be colorless as opposed to the pale green color observed for **2**. The cation species in **1** was found to be $\mathbf{BuGH}^+$ by structural analysis (vide infra); however, the protonated **BuG** species in **2** could not be identified.

IR and UV–vis-NIR spectroscopic analyses identified **3** and **5** as group **II** salts of fully ionic $F_nTCNQ^{\bullet-}$ and **4** and **6** as group **I** salts of $F_nTCNQ\text{-}OMe^-$ contaminated with small amount of $F_nTCNQ^{\bullet-}$ species (Supporting Information Figures S3–S6). The lowest absorption bands of **3** and **5** appear at an energy region higher than those of $K^+F_nTCNQ^{\bullet-}$ (8.2×10^3 vs 6.3×10^3 cm^{-1} for $n = 2$, and 9.3×10^3 vs 7.0×10^3 cm^{-1} for $n = 1$) and show marked broadening. These observations indicate the dimerized nature of $F_nTCNQ^{\bullet-}$ molecules in the segregated stack.

Crystal Structures of 1, 3, and 5: Protonated Site. It is known that the bond angle C5–N7–C8 of 9-alkyl-substituted **G** derivatives (θ in Scheme 3) is somewhat sensitive to protonation of **G** at the N7 position in comparison with the other angles (Supporting Information Table S2).[21e,27–29] Table 4 summarizes the θ values of **BuG** species in neutral, $F_nTCNQ^{\bullet-}$ salts (**1**, **3**, and **5**), 9-ethylguanine (**EtG**),[27] and protonated **EtG** ($\mathbf{EtGH}^+$).[28] Neutral **EtG** and **BuG** exhibit θ values in the range of 101.8–106.0°, while $\mathbf{EtGH}^+$ exhibits θ values in the range of 107.1–107.3° because of protonation. The θ values for **1** and **3** are 107.8° and 108.2°, respectively, clearly indicating protonation at the N7 position. There are two kinds of different values for θ in **5**; 104.0° and 107.7°; hence, the former is assigned to the more neutral species and the latter to the more protonated one at N7, in the hemiprotonated $(\mathbf{BuG})(\mathbf{BuGH}^+)$ species.

dx.doi.org/10.1021/cg400059h | Cryst. Growth Des. 2013, 13, 2778–2792

Table 4. C5−N7−C8 Bond Angles (θ) of Neutral and Protonated 9-Alkyl G Derivatives

compound	molecule	θ (deg)	ref
BuG	A	104.0(6)	this work
	B	101.8(6)	
	C	106.0(6)	
1, (**BuGH**$^+$)($F_4TCNQ^{\bullet-}$)	**BuGH**$^+$	107.8(2)	this work
3, (**BuGH**$^+$)($F_2TCNQ^{\bullet-}$)(MeOH)	**BuGH**$^+$	108.2(4)	this work
5, (**BuG**)(**BuGH**$^+$)($F_1TCNQ^{\bullet-}$)	**BuG**	104.0(2)	this work
	BuGH$^+$	107.7(2)	
EtG	A	104.8	27
	B	104.0	
(**EtGH**$^+$)($HCOO^-$)	A	107.1(2)	28
	B	107.3(2)	

Ionicity of F_nTCNQ. In Table 5, the C−C bond lengths of the F_nTCNQ molecule (a−d, Scheme 5) of salts **1**, **3**, and **5** are compared with those of neutral and fully ionized F_nTCNQ species,[30−33] although the data of fully ionized $F_1TCNQ^{\bullet-}$ has not been reported. In salt **1**, all a−d bond lengths except one of the d bonds (1.430 Å) are consistent with those in the fully ionized state,[31] which is in good agreement with the characterizations by IR and UV−vis-NIR spectra. Although the variation between each of the a−d bond lengths even in F_nTCNQ molecules is large, a similar tendency can be observed for the compounds where n = 2 and 1 (Table 5).[32,33] The charge of a TCNQ moiety (ρ) can be estimated from the C−C bond lengths using Kistenmacher's equation,[34] $\rho = -(r - r^0)/(r^1 - r^0)$, where $r = c/(b + d)$, and r^0 and r^1 are the values calculated for neutral and fully ionized TCNQ molecules, respectively. The ρ values of **1** and **3** estimated by this method are −0.95 and −1.17, respectively, which are similar to those for (Bu_4N^+)($F_4TCNQ^{\bullet-}$) and ($TTF^{\bullet+}$)($F_2TCNQ^{\bullet-}$) (ρ = −1), suggesting the fully ionized state of F_nTCNQ moieties. Although earlier studies of the crystal structures of fully ionized $F_1TCNQ^{\bullet-}$ are not accessible, the r value of **5** (0.498) being close to 0.5 strongly indicates the fully ionized state of the acceptor moiety.

Scheme 5. Bonds a−d in the F_nTCNQ Molecule

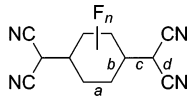

Salt 1 (BuGH$^+$)($F_4TCNQ^{\bullet-}$). Figure 5 shows the molecular structures of crystallographically independent one **BuGH**$^+$ and one $F_4TCNQ^{\bullet-}$ molecules with the atom labeling scheme.

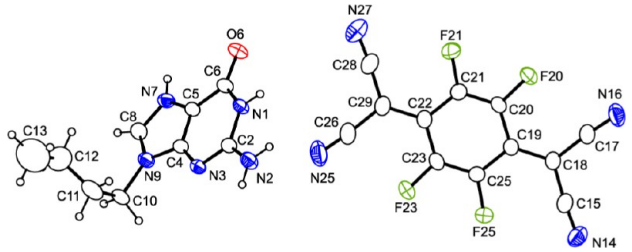

Figure 5. Molecular structures of **BuGH**$^+$ and $F_4TCNQ^{\bullet-}$ in **1** with the atom labeling scheme.

Figure 6 illustrates the packing of **BuGH**$^+$ molecules viewed along the c axis, where six **GH**$^+$ (**GH**$^+$ is the π-segment of a **BuGH**$^+$ molecule) columns are depicted, and n-butyl groups are allocated between columns 1 and 2, 3 and 4, and 5 and 6 with a period of 10.9 Å. Two **BuGH**$^+$ molecules form a dimer (red ellipses in Figure 6 except n-butyl groups) by the double complementary H-bonds (amine N2−H···N3, 2.99 Å, red dotted lines) having no net dipole, and each dimer is connected to the neighboring four dimers by N5−H···O6 H-bonds (2.73 Å, red dotted lines; for example, dimer ① is linked to dimers

Table 5. Bond Lengths of F_nTCNQ Molecules (a−d (Å))

compound	a (Å)	b (Å)	c (Å)	d (Å)	r[a]	ρ[b]	ref
F_4TCNQ	1.334	1.436	1.372	1.435	0.478	0	30
(Bu_4N^+)($F_4TCNQ^{\bullet-}$)	1.357	1.415	1.418	1.425	0.499	−1	31
1	1.354(4)	1.414(4)	1.411(4)	1.411(4)	0.498	−0.95	this work
(**BuGH**$^+$)($F_4TCNQ^{\bullet-}$)	1.348(4)	1.417(4)	1.411(4)	1.417(4)			
		1.418(3)		1.418(4)			
		1.418(4)		1.430(4)			
F_2TCNQ	1.328	1.443	1.376	1.437	0.478	0	32a
($TTF^{\bullet+}$)($F_2TCNQ^{\bullet-}$)	1.331	1.417	1.414	1.414	0.496	−1	32b
	1.334	1.418	1.411	1.433			
		1.437		1.435			
		1.425		1.419			
3	1.345(5)	1.419(5)	1.417(5)	1.420(5)	0.499	−1.17	this work
(**BuGH**$^+$)($F_2TCNQ^{\bullet-}$)(MeOH)	1.347(5)	1.421(5)	1.420(5)	1.417(5)			
		1.429(5)		1.418(6)			
		1.416(5)		1.421(6)			
F_1TCNQ[c]	1.336	1.433	1.370	1.412	0.480	0	33
		1.429		1.430			
5	1.353(4)	1.428(4)	1.409(4)	1.423(5)	0.498	−1	this work
(**BuG**)(**BuGH**$^+$)($F_1TCNQ^{\bullet-}$)	1.363(4)	1.430(4)	1.416(4)	1.412(4)			
		1.405(4)		1.410(5)			
		1.424(4)		1.423(4)			

[a] $r = (b + d)/c$. [b] $\rho = -(r - r^0)/(r^1 - r^0)$, where r^0 and r^1 are the values calculated for neutral and fully ionized F_nTCNQ. [c] Owing to the disorder of F atoms, the result was of poor quality ($R \approx 10\%$).

dx.doi.org/10.1021/cg400059h | Cryst. Growth Des. 2013, 13, 2778−2792

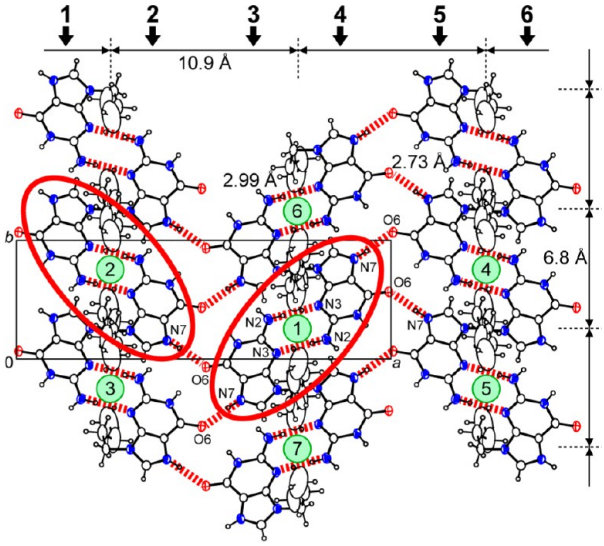

Figure 6. Polycationic layer of **1** viewed along the *c* axis. **BuGH**$^+$ columns 1−6 form a 2D polycationic layer. The red ellipse shows **BuGH**$^+$ dimers except *n*-butyl groups. Red dotted lines indicate H-bonds between **BuGH**$^+$ molecules with bond length (Å).

②−⑤ in Figures 6 and S7), forming a 2D polycationic layer in the *ab* plane (**GH**$^+$ layer = thickness of 4.2 Å) with *n*-butyl groups protruding up and down.

One C≡N group of $F_4TCNQ^{\bullet-}$ is attached to the cationic template by a H-bond with amine N2−H (N−H···N16≡C, 2.93 Å), and molecular long axis of $F_4TCNQ^{\bullet-}$ molecule is nearly parallel to the *c* axis (Figures 7 and 8). Thus, $F_4TCNQ^{\bullet-}$

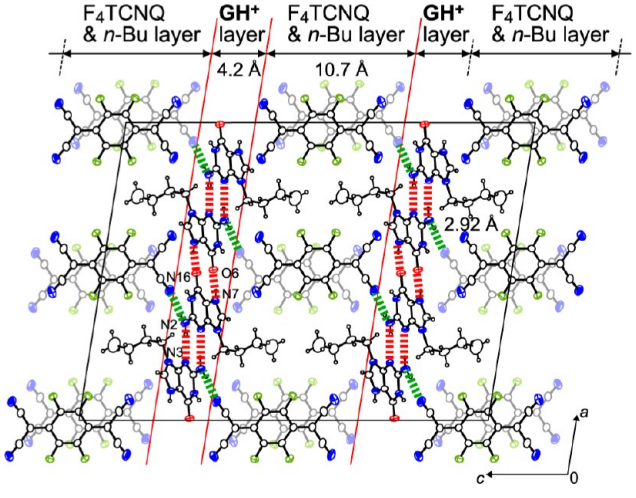

Figure 7. Crystal structure of **1** viewed along the *b* axis. Red and green dotted lines indicate H-bonds between **BuGH**$^+$ molecules and those between **BuGH**$^+$ and $F_4TCNQ^{\bullet-}$, respectively. Red lines are guides to eyes separating **GH**$^+$ and F_4TCNQ layers.

molecules form a segregated 1D column along the *b* axis according to the periodic pattern of the H-bond donating site (N2 atom, 6.8 Å intervals) in the polycationic template.

Although there is no short contact between the 1D F_4TCNQ columns along the *a* axis owing to the intrusion of *n*-butyl groups, F_4TCNQ molecules form a thick layer (thickness of 10.7 Å) in the *ab* plane, and the $F_4TCNQ^{\bullet-}$ and **GH**$^+$ layers alternate along the *c* axis (Figures 7 and 8). Within a column, F_4TCNQ molecules are dimerized, where the molecules slip

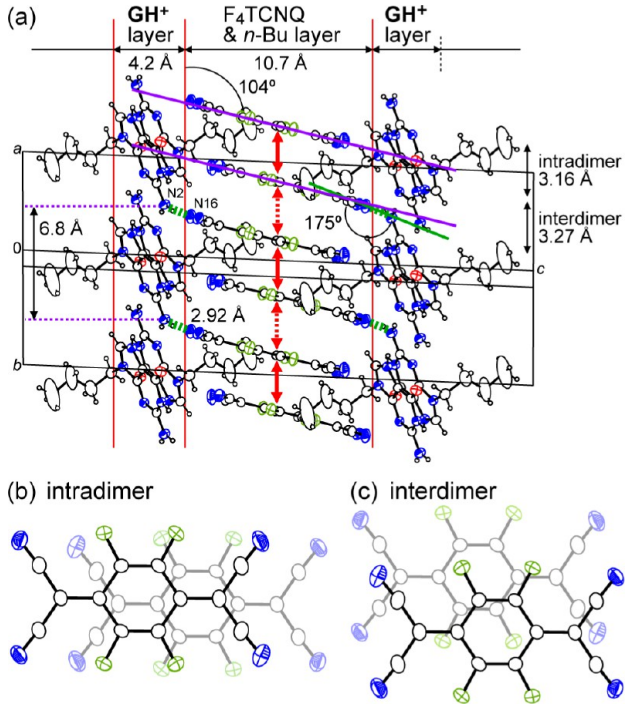

Figure 8. (a) Crystal structure of **1** viewed approximately along the [110] direction showing the relative orientation of the 2D polycationic template of **BuGH**$^+$ and $F_4TCNQ^{\bullet-}$ molecules. Red lines are guides to eyes separating **GH**$^+$ and F_4TCNQ layers. Purple lines show the molecular long axis of $F_4TCNQ^{\bullet-}$. Green dotted lines represent H-bonds between **BuGH**$^+$ and $F_4TCNQ^{\bullet-}$ molecules, respectively. Purple dotted lines and black arrow indicate the periodicity of N2 sites of **BuGH**$^+$ along the *b* axis. Red solid and dotted arrows represent intra- and interdimer interactions of $F_4TCNQ^{\bullet-}$ dimers. (b and c) Intra- and interdimer overlap patterns, respectively.

along the molecular long axis for intradimer stacking (Figure 8b) and along the molecular short axis for interdimer stacking (Figure 8c). The intra- and interdimer face-to-face separations are 3.16 and 3.27 Å, respectively (Figure 8a), and the overlap integrals are 22.35×10^{-3} and 3.27×10^{-3}, respectively. Broadening of the intermolecular CT band around 7.5×10^3 cm^{-1} in the UV−vis-NIR spectrum (Figure 4) is consistent with the dimerization feature. The fully ionic valence state and strong dimerization feature of $F_4TCNQ^{\bullet-}$ give rise to a spin-singlet insulator (room temperature conductivity $<10^{-7}$ S cm^{-1}).

Salt 3 (BuGH$^+$)($F_2TCNQ^{\bullet-}$)(MeOH). A crystallographically independent unit includes one molecule each of **BuGH**$^+$, $F_2TCNQ^{\bullet-}$, and MeOH (Figure 9a). The N7 atom of a **BuG** molecule is protonated to give **BuGH**$^+$, which then forms a H-bonded dimer by double complementary H-bonds (red dotted lines in Figure 9b; amine N2−H···N3, 3.06 Å), where the dipoles of **BuGH**$^+$ cancel out each other. Each dimerized **G** skeleton (indicated by the red ellipse) forms an infinite 1D ribbon with ∼8 Å in width (except the *n*-butyl groups) established by formation of MeOH-mediated H-bonds (orange dotted lines in Figure 9b; N7−H···O(MeOH), 2.77 Å, and O(MeOH)−H···O6, 2.73 Å).

Figure 10a demonstrates that *π*-stacking dimers of $F_2TCNQ^{\bullet-}$ (encircled by red dotted ellipses) with an interplanar distance of 3.16 Å (overlap integral = -25.99×10^{-3}) and an H-bonded dimer unit of **BuGH**$^+$ are alternately aligned along the *b* axis. They form a 1D *π*-column in which

dx.doi.org/10.1021/cg400059h | Cryst. Growth Des. 2013, 13, 2778−2792

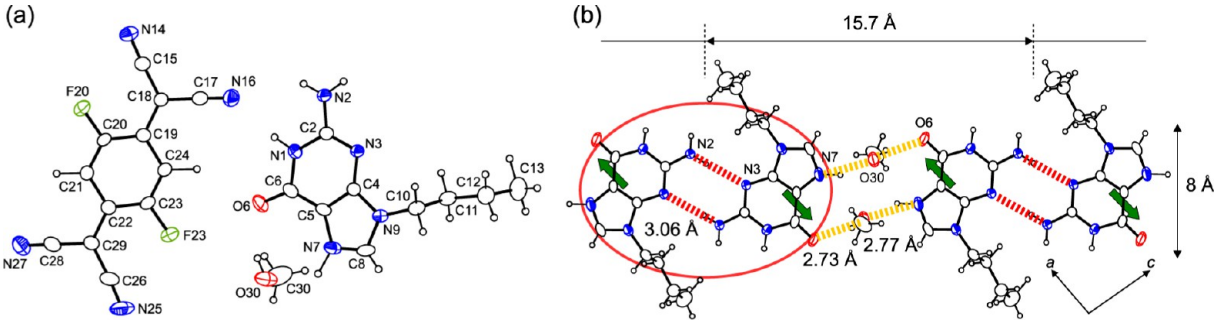

Figure 9. (a) Molecular structures of **3** with the atom labeling scheme. (b) H-bonded 1D ribbon of **BuGH**$^+$ in **3** parallel to the $[10\bar{1}]$ direction (H-bonds are mediated by MeOH). The red ellipse shows a **BuGH**$^+$ dimer except *n*-butyl groups $(\mathbf{GH}^+)_2$ with complementary double H-bonds. Red and orange dotted lines show H-bonds with bond lengths (Å). Green arrows indicate the dipole.

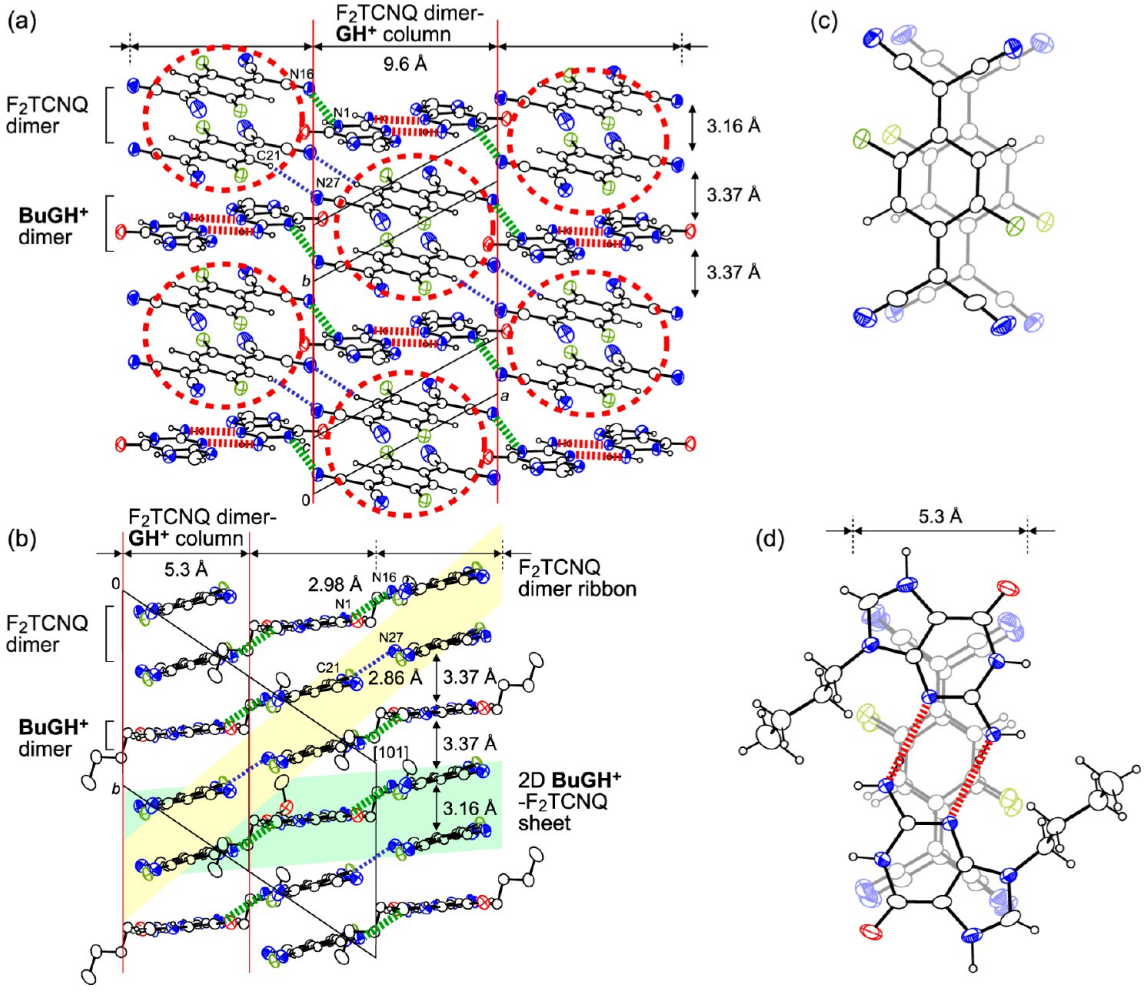

Figure 10. (a) Crystal structure of **3** viewed approximately along the *c* axis ($z = 0$) showing the stacking pattern in the $(\mathbf{GH}^+)_2(\mathrm{A}^{\bullet-})(\mathrm{A}^{\bullet-})$ column and the intercolumnar H-bonds (A = F_2TCNQ). F_2TCNQ$^{\bullet-}$ dimers are encircled by red dotted ellipses. (b) The stacking structure of **3** viewed along the $[10\bar{1}]$ direction showing the 1D F_2TCNQ$^{\bullet-}$ dimer ribbon (yellow sheet) and 2D **BuGH**$^+$–F_2TCNQ$^{\bullet-}$ sheet (green sheet). (c) Overlap pattern of the F_2TCNQ$^{\bullet-}$ dimer, and (d) overlap pattern of the H-bonded **BuGH**$^+$ dimer and the F_2TCNQ$^{\bullet-}$ dimer. Green, blue, and red dotted lines in panels a, b, and d indicate the H-bonds between **BuGH**$^+$ and F_2TCNQ$^{\bullet-}$, those between F_2TCNQ$^{\bullet-}$ molecules, and those within a **BuGH**$^+$ dimer, respectively.

$(\mathbf{GH}^+)_2(\mathrm{A}^{\bullet-})(\mathrm{A}^{\bullet-})$ is a repeating π-unit (A = F_2TCNQ) as shown in Figures 10a and 10b. Figure 10c shows the eclipsed overlap pattern within a F_2TCNQ$^{\bullet-}$ dimer that is sandwiched between **BuGH**$^+$ dimers along the *b* axis (Figure 10d) indicating a suitable size and shape match between the π-skeletons of the **BuGH**$^+$ dimer and F_2TCNQ molecule. The interplanar distance between the π-moieties of the **BuGH**$^+$ dimer and F_2TCNQ$^{\bullet-}$ is 3.37 Å.

Adjacent F_2TCNQ dimers are linked through C21–H···N27≡C H-bonds (2.86 Å, slightly longer than the sum of vdW radii,[24] overlap integral = -1.27×10^{-5}) to form a 1D structure along the [021] direction (blue dotted lines on yellow sheet in Figures 10b and 11a). The MeOH-mediated **BuGH**$^+$

dx.doi.org/10.1021/cg400059h | *Cryst. Growth Des.* 2013, 13, 2778–2792

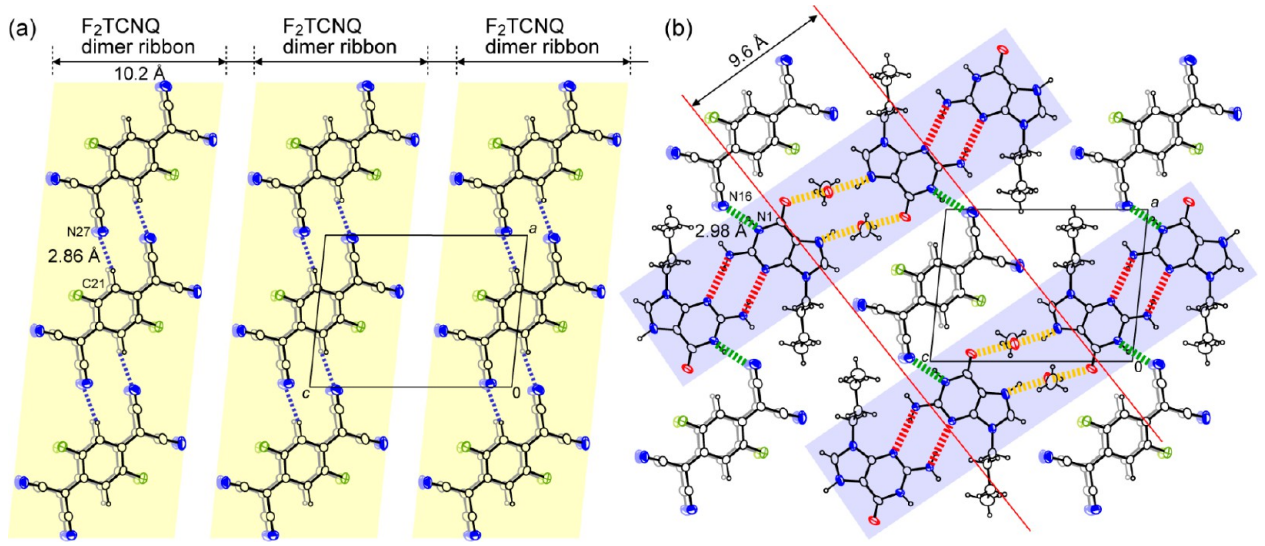

Figure 11. (a) Packing of $F_2TCNQ^{\bullet-}$ molecules of **3** viewed along the *b* axis showing the $F_2TCNQ^{\bullet-}$ dimer ribbons (yellow sheets) by C−H···N≡C bonds (blue dotted lines) extending along the [021] direction. (b) 2D **BuGH**$^+$−$F_2TCNQ^{\bullet-}$ sheet structure composed of MeOH mediated **BuGH**$^+$ ribbons (blue sheets) and dimers of $F_2TCNQ^{\bullet-}$ viewed along the *b* axis. Red, orange, and green dotted lines indicate H-bonds with bond lengths (Å) within a **BuGH**$^+$ dimer, between **BuGH**$^+$ and MeOH molecules, and between **BuGH**$^+$ and $F_2TCNQ^{\bullet-}$ molecules, respectively. Two red lines are guides for indicating that the size of the F_2TCNQ molecule approximately corresponds to the distance between two **BuGH**$^+$ molecules linked to MeOH molecules.

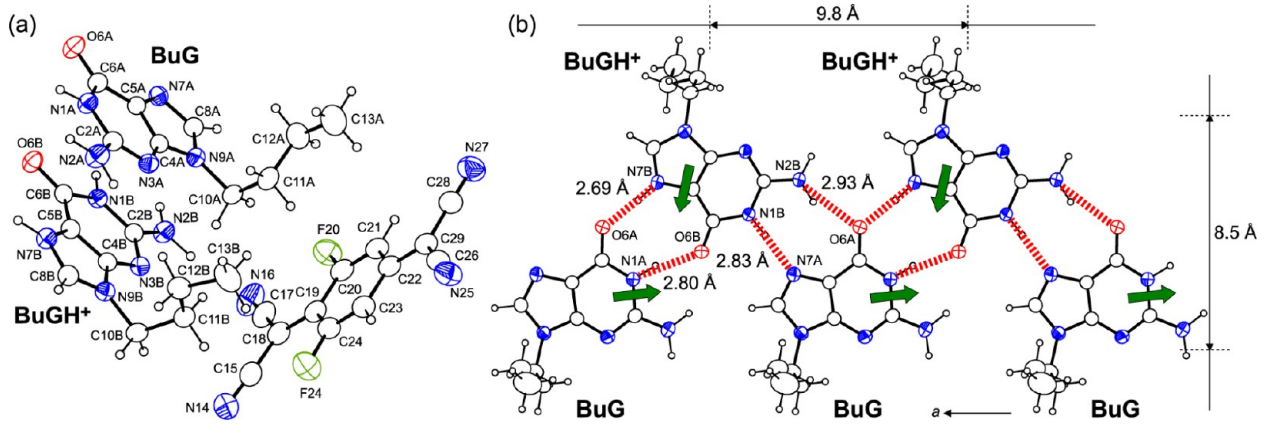

Figure 12. (a) Molecular structures of component molecules in (**BuG**)(**BuGH**$^+$)($F_1TCNQ^{\bullet-}$) (**5**) showing the atom labeling scheme. F20 and F24 atoms are disordered in a 0.64:0.36 ratio. (b) H-bonded infinite 1D ribbon of (**BuG**)(**BuGH**$^+$) in **5**. Red dotted lines show the H-bonds with bond lengths (Å). Green arrows indicate the dipole of **BuG** and **BuGH**$^+$.

ribbons (blue sheets in Figure 11b) and F_2TCNQ dimers are connected by the N1−H···N16≡C H-bonds (2.98 Å) to form a 2D sheet (green sheets and green dotted lines in Figures 10b and 11b, respectively). This salt gradually loses crystal solvents, and thus, the measurements of physical properties (magnetic susceptibility and electrical conductivity) could not be performed. However, it is anticipated that dimerization of radical spins of $F_2TCNQ^{\bullet-}$ results in an electric insulating nature.

Salt 5 (BuG)(BuGH$^+$)(F_1TCNQ$^{\bullet-}$). Three types of molecules, neutral **BuG**, protonated **BuGH**$^+$, and $F_1TCNQ^{\bullet-}$, are crystallographically independent (Figure 12a). The F atom in F_1TCNQ is disordered, appearing at two positions in the ratio of 0.64:0.36. **BuG** and **BuGH**$^+$ are connected through complementary double H-bonds, amine N2B−H···O6A (2.93 Å), and amide N1B−H···N7A (2.83 Å), N7B−H···O6A (2.69 Å) and N1A−H···O6B (2.80 Å) (red dotted lines in Figure 12b), establishing an infinite flat 1D ribbon of hemiprotonated (**BuG**)(**BuGH**$^+$) (width except *n*-butyl groups, 8.5 Å) along the *a* axis.

The H-bonded (**BuG**)(**BuGH**$^+$) ribbons stack along the *b* axis to form a 2D polycationic layer in the *ab* plane (blue sheet in Figure 13), where two types of overlap patterns for the ribbons (Types A and B, Supporting Information Figure S8) with interplanar distances of 3.31 and 3.27 Å, respectively, are observed. Each ribbon has an infinite dipole; however, the neighboring ribbon in the π-stack has the dipole in the opposite direction, canceling out individual dipoles in the crystal.

As shown in Figure 13, the 2D layer of π-moieties of the (**BuG**)(**BuGH**$^+$) ribbons (blue sheets; thickness, 5.4 Å) and $F_1TCNQ^{\bullet-}$ layers (red sheets; thickness, 11.7 Å) alternately stack along the *c* axis. The $F_1TCNQ^{\bullet-}$ layer includes *n*-butyl groups of **BuG** and **BuGH**$^+$ molecules. F_1TCNQ forms a face-to-face dimer with an interplanar distance of 3.23 Å (Figure 14a). The F_1TCNQ dimers are connected to each other through short C21−H···N27≡C H-bonds (2.67 Å, blue dotted

dx.doi.org/10.1021/cg400059h | *Cryst. Growth Des.* 2013, 13, 2778−2792

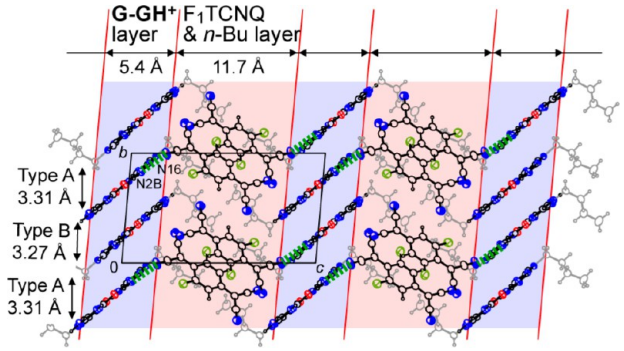

Figure 13. Crystal structure of **5** viewed along the *a* axis. Blue sheets include the π-moieties of a (**BuG**)(**BuGH**$^+$) layer, while red sheets include F_1TCNQ and *n*-butyl groups. Green dotted lines are H-bonds between (**BuG**)(**BuGH**$^+$) and $F_1TCNQ^{\bullet-}$ molecules. Red lines are guides to eyes separating a layer of **G**−**GH**$^+$ from layers of F_1TCNQ and *n*-butyl group.

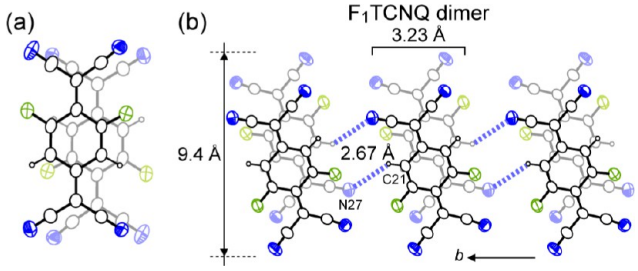

Figure 14. (a) Overlap pattern of the F_1TCNQ molecules of **5** in a dimer. (b) 1D array of F_1TCNQ dimers supported by C−H···N≡C H-bonds (blue dotted lines) extending along the *b* axis.

lines in Figure 14b) to form a 1D ribbon along the *b* axis. The adjacent ribbons of F_1TCNQ dimers are nearly separated from each other by *n*-butyl groups along the *a* axis (Figure 15). The intradimer overlap integral of $F_1TCNQ^{\bullet-}$ is -18.98×10^{-3}, and the interdimer overlap integrals are calculated as -8.08×10^{-5} and -2.79×10^{-6} along the side-by-side direction (*b* axis) and face-to-face direction (*a* axis), respectively.

The F_1TCNQ dimer ribbons are linked to the (**BuG**)-(**BuGH**$^+$) ribbons by N2B−H···N16≡C H-bonds (3.04 Å, green dotted lines in Figures 13 and 15), constructing a 3D architecture (Supporting Information Figure S9). Consistent with the fully ionic state, the solid is insulating (room temperature conductivity $<10^{-8}$ S cm^{-1}), and most spins are magnetically quenched by the strong antiferromagnetic coupling between $F_1TCNQ^{\bullet-}$ molecules within a dimer (only ~9% of the total of noninteracting $S = 1/2$ spins are active at 300 K).[22]

H-Bonded Architectures of BuG and Their Role as Template. In this section, the motifs representing the H-bond connectivity and relative position of **BuG** and/or **BuGH**$^+$ molecules in the crystals of neutral **BuG**, and salts **1**, **3**, and **5** are examined to determine how **BuG** species form supramolecular architectures to establish templates for the counter molecules.

Scheme 6 illustrates several reported H-bonding patterns of **G** pairs of N^9-substituted derivatives, by classifying the manner of connectivity and relative positioning. Alternation of Type 1 and Type 2 H-bonds, in which the dipoles of each **G** molecule are canceled out, forms a 1D ribbon structure (Ribbon-B in Scheme 2b).[35] Type 3 H-bonds are observed in the cyclic **G**-

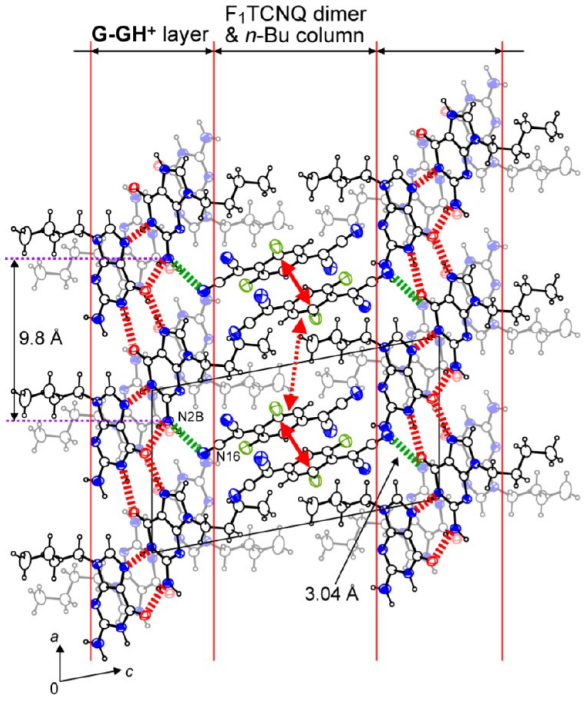

Figure 15. Crystal structure of **5** viewed along the *b* axis. Green and red dotted lines show the H-bonds between **BuGH**$^+$ and $F_1TCNQ^{\bullet-}$ (amino N2B−H···N16≡C) and those between **BuG** and **BuGH**$^+$, respectively. Purple dotted lines and black arrow in (a) show the periodicity of N2 sites of **BuGH**$^+$ within a (**BuG**)(**BuGH**$^+$) ribbon along the *a*-axis. Red lines in panel b are guides to eyes for separating a layer of **G**−**GH**$^+$ from layers of F_1TCNQ and *n*-butyl group. Red solid and dotted arrows represent intra- and interdimer interactions of $F_1TCNQ^{\bullet-}$ dimers, respectively.

quartet.[36] In the case of Type 4 H-bonds, the dipoles are not quenched completely, and the 1D ribbon of these **G** pairs possesses a large dipole along the chain direction (Ribbon-A in Scheme 2a).[35,37]

Neutral BuG. In the crystal structure of **BuG**, 1D ribbons of Type 4 pairing are observed (A-ribbon and BC-ribbon in Figures 2a and 2b, respectively). The N2A−H···O6B H-bonds (purple dotted lines in Figures 2e−2f) between the A-ribbon and π-dimer of BC-ribbons, which are perpendicular to each other, generate a 3D network structure (Supporting Information Figure S1). A similar 3D network has been observed in the crystal structure of **EtG** in which both ribbons running perpendicular to each other exhibit the π-dimerization feature like the BC-ribbon in **BuG**.[27]

Protonated G. Protonation at the N7 atom increases the variation of H-bonding motifs (Types 5−7 in Scheme 6). In Type 5 paring, the dipoles of **GH**$^+$ are canceled out.[38] Alternation of Types 2 and 5 pairing establishes a 1D ribbon structure.[29] The coexistence of **G** and **GH**$^+$ species gives the Type 7 H-bond (N7−H···N7, Scheme 6), which links pairs of Type 2 H-bonds forming a 1D ribbon as shown in Scheme 2f.[21d,e] In some cases, these **GH**$^+$ ribbons stack to form a 2D layer structure,[39] in which the anion species are linked to the cationic template by H-bonds and are arranged in a 2D motif between the **GH**$^+$ layers. Figure 16 shows redrawn motifs of the H-bonded ribbon structures of **3** (a), **5** (b), and **1** (c) with H-bonding connectivities. The positive site in a **BuGH**$^+$ molecule is represented by the symbol ⊕.

dx.doi.org/10.1021/cg400059h | Cryst. Growth Des. 2013, 13, 2778−2792

Scheme 6. H-Bonding Patterns of G Pairs in Neutral and Protonated States

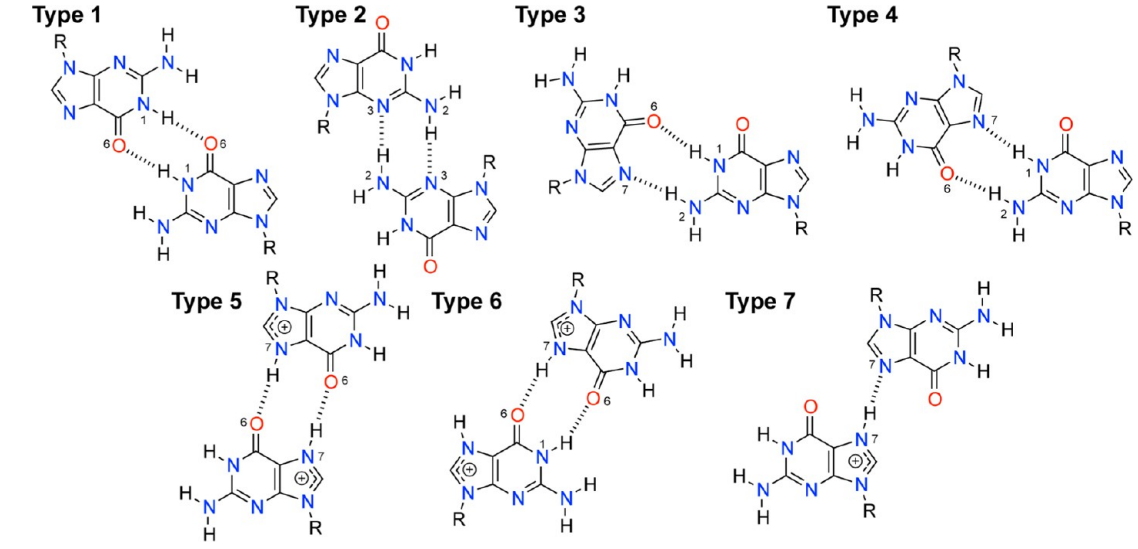

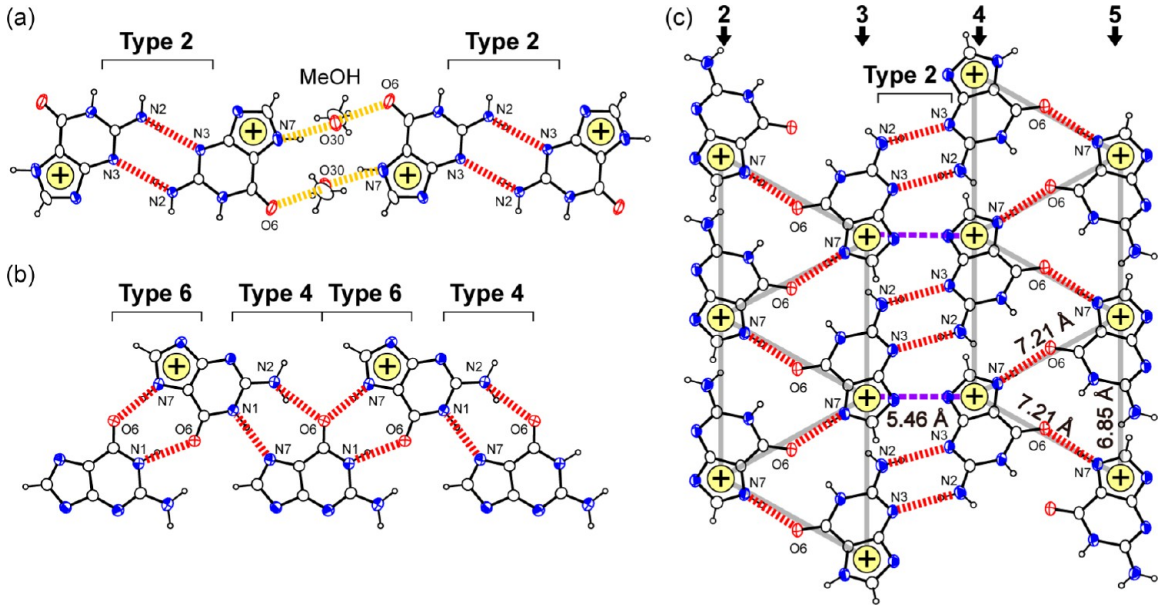

Figure 16. Motifs of H-bonded ribbons of (a) **3**, (b) **5**, and (c) **1** (only columns 2−5 in Figure 6 are depicted). Types 2, 4, and 6 are the H-bonding patterns depicted in Scheme 6. The symbol ⊕ represents the postulated positive site in **BuGH**$^+$ as a point charge. The *n*-butyl groups are omitted for simplicity. Gray lines and purple lines in (c) represent the isosceles triangular cationic lattice formed by connecting the ⊕ symbols.

Salt 3. In salt **3**, **BuGH**$^+$ molecules form a dimer with the Type 2 H-bond pairing, and the dimers are connected by MeOH-mediated H-bonds (Figure 16a). Similar solvent-mediated 1D ribbon structures have been observed in the hydrate salts of protonated 9-methylguanine (**MeGH**$^+$) and **EtGH**$^+$.[40] The N1 sites of **BuGH**$^+$ molecules of **3** fixed the anion molecules by H-bonds (N1−H···N16≡C), in which MeOH participation is the key feature responsible for adjusting the separation between the N1 sites of the neighboring **BuGH**$^+$ dimers (see the two red lines in Figure 11b) to the separation observed between the N16 sites of the $F_2TCNQ^{\bullet-}$ dimers (9.6 Å). The H-bonded ribbons in **3** run parallel to the molecular long axis of the anion molecule.

Salt 5. In salt **5**, **BuG** and **BuGH**$^+$ molecules are alternately linked through H-bonds of Types 4 and 6 pairings to form a 1D ribbon structure (Figure 16b). One side of the ribbon is composed of only **BuGH**$^+$, and the opposite side includes neutral **BuG** species as well. The N2 sites of **BuGH**$^+$ species fix $F_1TCNQ^{\bullet-}$ molecules by H-bonds, and the period of the F_1TCNQ dimers is 9.8 Å, corresponding to that of N2 sites of **BuGH**$^+$ molecules within the 1D ribbon (black arrow in Figure 15).

The F_1TCNQ dimers are arranged via side-by-side C−H···N≡C H-bonds and via $\pi-\pi$ interactions along the *a*-axis, forming a 2D layer in the *ab* plane, which is sandwiched by the π-moieties of polycationic (**BuG**)(**BuGH**$^+$) layers (Figure 15). Therefore, the (**BuG**)(**BuGH**$^+$) ribbon functions as both a polycationic template and a wall forming a segregated layer with the $F_1TCNQ^{\bullet-}$ molecules.

Salt 1. Only salt **1** has a 2D polycationic network by Type 2 H-bond pairing and N7−H···O6 H-bonds (Figure 16c). A 2D sheet formed by similar H-bond motifs has also been observed in **MeGH**$^+$**Br**$^-$ salt.[41] The N2 atoms of **BuGH**$^+$ fixed the $F_4TCNQ^{\bullet-}$ molecules by N2−H···N≡C H-bonds with a

dx.doi.org/10.1021/cg400059h | *Cryst. Growth Des.* 2013, 13, 2778−2792

period of GH^+ pairs (6.8 Å, black arrow in Figure 8a). The $F_4TCNQ^{\bullet-}$ 1D column is sandwiched by the 2D layer of $BuGH^+$ with the dihedral angle of 104° between the $BuGH^+$ wall plane and the molecular long axis of $F_4TCNQ^{\bullet-}$ (Figure 8a). The *n*-butyl group array inhibits the side-by-side interactions of the $F_4TCNQ^{\bullet-}$ column.

Different connectivity and packing manner of the polycationic ribbons and anion molecules are noticed among salts **1**, **3**, and **5**; namely, ribbons of salt **3** grow parallel to the molecular long axis of the anion molecule (black arrows in Figure 11b), while the ribbon of salts **1** and **5** is directed such that it forms a large angle with the molecular long axis of the anion molecule (Figures 8a and 15). Both salts **1** and **5** have segregated columns of anion molecules, while in salt **3**, a dimer of anion molecules is sandwiched by $BuGH^+$ (Figure 10). Existence of segregated stacking of radical molecules is the first essential requirement for high conductivity of a metallic band structure or a Mott insulating state.

The cationic sites of the 2D sheet in Figure 16c form a triangular lattice, which was achieved by connecting the ⊕ symbols. Each isosceles triangle is connected by sharing one side, 7.21 Å in length, along the *b* axis. Such a H-bonded $BuGH^+$ assembly may serve as a template for the molecular arrangement of various anion radical species to form a triangular zigzag spin chain via Coulomb interactions, that has become recently important as renewed spin frustrated system as found for CaV_2O_4, $Cu(ampy)Br_2$ (ampy = 2-(2-aminomethyl)pyridine), and $(VO)(SO_4)(bpy)$ (bpy = 2,2′-bipyridine).[42] Considering the fact that the triangular zigzag spin chain can transform to other geometrical spin systems such as 1D spin chain and two-leg spin ladder[43] by modifying the interunit interactions, the self-assembling nature of $BuGH^+$ is promising for the systematic exploration of various spin system. Especially, it is possible that the derivatization of guanine, which modifies the self-assembling structure, allows the modification of spin structures formed by anion radicals as counter species.

CONCLUSION

Structural template effect of a nucleobase derivative, **BuG**, in CT complexes was investigated in the **BuG**–F_nTCNQ system. The reaction between **BuG** and F_nTCNQ derivatives in a mixed solvent containing MeOH proceeded via generation of $F_nTCNQ\text{-}OMe^-$ to yield two types of salts, $F_nTCNQ\text{-}OMe^-$ (Group **I**) and fully ionic $F_nTCNQ^{\bullet-}$ (Group **II**) with protonated $BuGH^+$ species, as observed in **C**–TCNQ systems.[9] Structural analyses of the **BuG** and Group **II** salts revealed that **BuG** possesses a strong tendency to form 1D ribbon structures supported by robust complementary H-bonds in the neutral, hemiprotonated (**5**), and protonated states (**3**), and a H-bonded 2D sheet structure was also observed in **1**. The 1D ribbons of hemiprotonated $(BuG)(BuGH^+)$ in **5** further stacked owing to the π–π interaction to form a 2D layer. Although 2D layers were not formed in the crystals of **BuG** and salt **3**, the 1D ribbons observed in these crystals have the potential to form a 2D segregated layer, as shown in the literatures.[39−41] The fact that the H-bonded arrays in salts **1**, **3**, and **5** were linked with $F_nTCNQ^{\bullet-}$ through N–H···N≡C H-bonds indicates the high potential of $BuGH^+$ assemblies as structural templates for $TCNQ^{\bullet-}$ derivatives to fix and arrange anionic π-molecules periodically. Unfortunately, mixed-valence and highly conductive salts (Group **III**) could not be obtained in the **BuG**–F_nTCNQ system; however, further chemical modification of **G** to control the arrangement of GH^+ 1D ribbons will provide a favorable template for not only conductive but also magnetic CT solids.

EXPERIMENTAL SECTION

General. 2-Amino-6-chloropurine was used as purchased. F_nTCNQ derivatives were synthesized in our laboratory and were purified by sublimation. MeOH, MeCN, and 1,2-dichloroethane used for complex formation were distilled under an inert gas prior to use, and the reactions were performed under an inert atmosphere.

Synthesis of BuG. BuG was prepared according to the modified procedures in the literatures (Scheme 7).[44−46] Into a suspension of 2-amino-6-chloropurine **a** (26.6 g, 157 mmol) and K_2CO_3 (21.7 g, 157 mmol) in DMF (400 mL), 1-bromobutane (17.0 mL, 158 mmol) was added, and the mixture was stirred at room temperature for 2 days. The reaction mixture was diluted with brine, and then extracted with ethyl acetate. The organic extract was concentrated under reduced pressure. The resulting precipitate was collected by filtration, to give the crude product as a pale yellow powder (30.9 g). The precipitate (25.0 g) was subjected to silica gel column chromatography (hexane/ethyl acetate, 1:5) to give the pure product of 2-amino-9-*n*-butyl-6-chloropurine **b** (20.5 g, 87%) as a colorless solid (mp. 138−141 °C, lit. 138−140 °C[44]). Compound **b** (8.09 g, 36.0 mmol) was dissolved in 6 M aqueous HCl solution (360 mL), and the mixture was refluxed for 1 h. After cooling to room temperature, the solution was neutralized by an aqueous NaOH solution (33 wt %, 240 g) and a saturated aqueous Na_2CO_3 solution. The resulting precipitate was collected by filtration to give crude **BuG** (7.04 g) as a white powder. After it was dissolved in an aqueous NaOH solution (4 wt %, 85 mL), the crude product was treated with charcoal under reflux, and then the charcoal was then removed by filtration. The filtrate was neutralized by 3 M aqueous HCl solution. The resulting precipitate was collected by filtration, to give **BuG** (5.71 g, 77%) as a white powder. Further purification was performed by recrystallization from MeOH (1.7 L) to give colorless prisms (3.81 g, 51%). dec 321−326 °C (lit. mp. > 260 °C[46]); ^{1}H NMR (400 MHz, DMSO-d_6) δ 0.87 (t, 3H, J = 7.3 Hz), 1.18−1.27 (m, 2H), 1.64−1.72 (m, 2H), 3.91 (t, 2H, J = 7.2 Hz), 6.40 (s, 2H), 7.66 (s, 1H), 10.49 (s, 1H); EI-MS, m/z 207 (M^+, 29%); IR (KBr) 3478, 3292, 3153, 2958, 2931, 2874, 2822, 2710, 1693, 1630, 1606 cm^{-1}. Anal. Calcd. for $C_9H_{13}N_5O$: C, 52.16; H, 6.32; N, 33.79; O, 7.72%. Found: C, 51.79; H, 6.30; N, 33.92; O, 8.01%.

Scheme 7. Synthetic Procedure of BuG

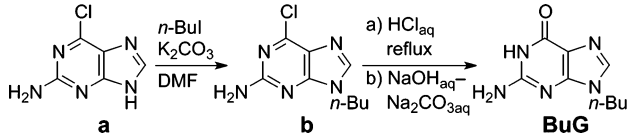

Preparation of F_nTCNQ Salts. *F_4TCNQ Salt* ***1***. In a 100-mL two-necked-modified round-bottomed flask, **BuG** (62.4 mg, 0.30 mmol) was dissolved in MeOH (50 mL) under reflux. To this solution, a solution of F_4TCNQ (150.4 mg, 0.55 mmol) in hot MeCN (40 mL) was added, and the reaction solution immediately turned green. After it was stirred for 5 min, the mixture was evaporated under reduced pressure, and the residual solid was suspended in MeCN (30 mL). The insoluble materials were removed by filtration, and the filtrate was concentrated under reduced pressure to ∼3 mL. After the addition of MeOH (2 drops), the solution was left standing at 5 °C to give **1** (16.0 mg, 11% from **BuG**) as dark blue crystals. dec 218−229 °C (gradually decomposed). Anal. Calcd. for $C_{21}H_{14}F_4N_9O$: C, 52.07; H, 2.91; N, 26.02; F, 15.69%. Found: C, 52.09; H, 2.82; N, 26.25; F, 15.59%.

F_2TCNQ Salt ***3***. In a 100-mL two-necked-modified round-bottomed flask, **BuG** (30.0 mg, 0.15 mmol) was dissolved in MeOH (40 mL) under reflux. To this solution, a solution of F_2TCNQ (140.0 mg, 0.58 mmol) in hot 1,2-dichloroethane (50 mL) was added, and the reaction solution gradually turned green. The mixture was evaporated under reduced pressure, and the residual solid was dissolved in MeOH (5

dx.doi.org/10.1021/cg400059h | *Cryst. Growth Des.* 2013, 13, 2778−2792

mL) at 50 °C. The solution was left standing at −18 °C for 2 days to give **3** (1.4 mg) as dark blue microcrystals. Cooling the filtrate at −18 °C for 4 days afforded additional **3** (7.5 mg, total 8.9 mg, 11% from **BuG**) as dark blue columnar crystals. Because of the efflorescence of **3** that caused decomposition of crystals, elemental analysis and measurements of physical properties (magnetic susceptibility and conductivity) could not be performed.

Measurements. ^{1}H NMR spectra were measured at 400 MHz on a JEOL JNM-FX400 spectrometer using DMSO-d_6 as the solvent and tetramethylsilane as an internal standard. The electron impact mass spectra (EI-MS) were measured with a Thermo Finnigan Trace DSQ. Elemental analyses were performed at the Center for Organic Elemental Microanalysis, Kyoto University. Melting points were measured with a Yanaco MP-500D micro melting-point apparatus and were not corrected. Measurements of absorption spectra were performed with a KBr disk on a Perkin-Elmer PARAGON 1000 Series FT-IR (resolution 2 or 4 cm^{-1}) for IR and near-IR regions (400−7800 cm^{-1}), and on a SHIMADZU UV-3100 spectrometer for near-IR, visible, and ultraviolet (UV−vis-NIR) regions (3800−42000 cm^{-1}). Electrical conductivity of the single crystal of **1** was measured with Keithley 2400 by two probe method. The 10 μm gold wires were attached to the crystal with gold paste as the electrodes.

Cyclic Voltammetry Measurement. Cyclic voltammetric measurements were performed using a solution of 0.1 M Bu_4NBF_4 in MeCN vs SCE on an ALS/chi Electrochemical Analyzer Model 650 A at room temperature. The experiments employed a Pt plate working electrode, a Pt wire counter electrode, and a SCE reference electrode.

X-ray Crystallography. The intensity data of the structural analysis were collected using an oscillator-type X-ray imaging plate (DIP-2020K) or a Rigaku Raxis-Rapid imaging plate using monochromated Mo Kα (0.71070 Å) or Cu Kα (1.54187 Å) radiation, respectively. The structures were solved by a direct method using SHELXS-97[47] or SIR-2004.[48] Refinements of structures were achieved by a full matrix least-squares method (SHELXL-97).[49] Positions of hydrogen atoms were determined by assuming an sp^2 or sp^3 configuration for each atom with an X−H (X = C, N, and O) distance of 1.0 Å. Parameters were refined by adopting anisotropic and isotropic temperature factors for non-hydrogen and hydrogen atoms, respectively.

Intermolecular overlap integrals between LUMOs of F_nTCNQ molecules were calculated on the bases of the crystal structures by the extended Hückel method with single ζ parameters.

■ ASSOCIATED CONTENT

Ⓢ Supporting Information

UV−vis-NIR and IR spectra of products of F_2TCNQ and F_1TCNQ, pictures of crystalline products, selected bond angles of **G** molecules in **BuG**, salts **1**, **3**, and **5**, and related compounds, and X-ray crystallographic data for each structure in CIF format. This material is available free of charge via the Internet at http://pubs.acs.org.

■ AUTHOR INFORMATION

Corresponding Author

*Tel: (+81)-52-838-2542. Fax: (+81)-52-833-7200. E-mail: tmurata0921@gmail.com (T.M.); gsaito@meijo-u.ac.jp (G.S.).

Notes

The authors declare no competing financial interest.

■ ACKNOWLEDGMENTS

This work was supported in part by a Grant-in-Aid for Scientific Research (S) (23225005) from the Ministry of Education, Culture, Sports, Science, and Technology, Japan.

■ REFERENCES

(1) Fink, H.-W.; Schönenberger, C. *Nature* **1999**, *398*, 407−410.
(2) Porath, D.; Bezryadin, A.; de Vries, S.; Dekker, C. *Nature* **2000**, *403*, 635−638.
(3) Tran, P.; Alavi, B.; Gruner, G. *Phys. Rev. Lett.* **2000**, *85*, 1564−1567.
(4) Kasumov, A. Y.; Kociak, M.; Guéron, S.; Reulet, B.; Volkov, V. T.; Klinov, D. V.; Bouchiat, H. *Science* **2001**, *291*, 280−282.
(5) (a) Jeffrey, G. A.; Saenger, W. *Hydrogen Bonding in Biological Structures*; Springer: Berlin, 1991. (b) Sivakova, S.; Rowan, S. J. *Chem. Soc. Rev.* **2005**, *34*, 9−21. (c) Sessler, J. L.; Jayawickramarajah, J. *Chem. Commun.* **2005**, 1939−1949. (d) Sessler, J. L.; Lawrence, C. M.; Jayawickramarajah, J. *Chem. Soc. Rev.* **2007**, *36*, 314−325.
(6) Fourmigué, M.; Batail, P. *Chem. Rev.* **2004**, *104*, 5379−5418.
(7) (a) Yamochi, H.; Komatsu, T.; Matsukawa, N.; Saito, G.; Mori, T.; Kusunoki, M.; Sakaguchi, K. *J. Am. Chem. Soc.* **1993**, *115*, 11319−11327. (b) Horiuchi, S.; Yamochi, H.; Saito, G.; Sakaguchi, K.; Kusunoki, M. *J. Am. Chem. Soc.* **1996**, *118*, 8604−8622. (c) Murata, T.; Morita, Y.; Yakiyama, Y.; Fukui, K.; Yamochi, H.; Saito, G.; Nakasuji, K. *J. Am. Chem. Soc.* **2007**, *129*, 10837−10846. (d) Saito, G.; Yoshida, Y. *Bull. Chem. Soc. Jpn.* **2007**, *80*, 1−137. (e) Baudron, S. A.; Avarvari, N.; Batail, P.; Coulon, C.; Clérac, R.; Canadell, E.; Auban-Senzier, P. *J. Am. Chem. Soc.* **2003**, *125*, 11583−11590. (f) Baudron, S. A.; Batail, P.; Coulon, C.; Clérac, R.; Canadell, E.; Laukhin, V.; Melzi, R.; Wzietek, P.; Jérome, D.; Auban-Senzier, P.; Ravy, S. *J. Am. Chem. Soc.* **2005**, *127*, 11785−11797.
(8) (a) Morita, Y.; Maki, S.; Ohmoto, M.; Kitagawa, H.; Okubo, T.; Mitani, T.; Nakasuji, K. *Org. Lett.* **2002**, *4*, 2185−2188. (b) Morita, Y.; Miyazaki, E.; Umemoto, Y.; Fukui, K.; Nakasuji, K. *J. Org. Chem.* **2006**, *71*, 5631−5637. (c) Murata, T.; Umemoto, Y.; Miyazaki, E.; Nakasuji, K.; Morita, Y. *CrystEngComm* **2012**, *14*, 6881−6887. (d) Murata, T.; Miyazaki, E.; Maki, S.; Umemoto, Y.; Ohmoto, M.; Nakasuji, K.; Morita, Y. *Bull. Chem. Soc. Jpn.* **2012**, *85*, 995−1006.
(9) Neilands, O. *Mol. Cryst. Liq. Cryst.* **2001**, *355*, 331−349.
(10) (a) Murata, T.; Saito, G.; Nishimura, K.; Enomoto, Y.; Honda, G.; Shimizu, Y.; Matsui, S.; Sakata, M.; Drozdova, O. O.; Yakushi, K. *Bull. Chem. Soc. Jpn.* **2008**, *81*, 331−344. (b) Murata, T.; Enomoto, Y.; Saito, G. *Solid State Sci.* **2008**, *10*, 1364−1368. (c) Sakata, M.; Maesato, M.; Miyazaki, T.; Nishimura, K.; Murata, T.; Yamochi, H.; Saito, G. *J. Phys.: Conf. Ser.* **2008**, *132*, 012011/1−4.
(11) Yoshida, Y.; Maesato, M.; Ishikawa, M.; Nakano, Y.; Hiramatsu, T.; Yamochi, H.; Saito, G. *Chem.—Eur. J.* **2013**, in press.
(12) (a) *Semiconductors and Semimetals: Highly Conducting Quasi-One-Dimensional Organic Crystals*; Conwell, E. M., Ed.; Academic Press: New York, 1988; Vol. 27. (b) Ishiguro, T.; Yamaji, K.; Saito, G. *Organic Superconductors*, 2nd ed.; Springer-Verlag: Berlin, 1998. (c) Jérome, D.; Schulz, H. J. *Adv. Phys.* **1982**, *31*, 299−490.
(13) Seidel, C. A. M.; Schulz, A.; Sauer, M. H. M. *J. Phys. Chem.* **1996**, *100*, 5541−5553.
(14) Wetmore, S. D.; Boyd, R. J.; Eriksson, L. A. *Chem. Phys. Lett.* **2000**, *322*, 129−135 and references therein..
(15) Berlinsky, A. J.; Carolan, J. F.; Weiler, L. *Can. J. Chem.* **1974**, *52*, 3373−3377.
(16) *Data for Biochemical Research*, 3rd ed.; Dawson, R. M. C., Elliot, W. H., Jones, K. M., Eds.; Clarendon Press: Oxford, U.K., 1986.
(17) Davis, J. T.; Spada, G. P. *Chem. Soc. Rev.* **2007**, *104*, 296−313.
(18) (a) Jeffrey, G. A.; Kinoshita, Y. *Acta Crystallogr.* **1963**, *16*, 20−28. (b) Barker, D. L.; Marsh, R. E. *Acta Crystallogr.* **1964**, *17*, 1581−1587.
(19) Hulme, A. T.; Tocher, D. A. *Cryst. Growth Des.* **2006**, *6*, 481−487 and references therein..
(20) (a) Fujinami, F.; Ogawa, K.; Arakawa, Y.; Shirotake, S.; Fujii, S.; Tomita, K. *Acta Crystallogr.* **1979**, *B35*, 968−970. (b) Salam, Md. A.; Aoki, K. *Inorg. Chim. Acta* **2000**, *311*, 15−24. (c) Armentano, D.; De Munno, G.; Rossi, R. *New J. Chem.* **2006**, *30*, 13−17. (d) García-Terán, J. P.; Castillo, O.; Luque, A.; García-Couceiro, U.; Beobide, G.; Román, P. *Cryst. Growth Des.* **2007**, *7*, 2594−2600.
(21) (a) Metzger, S.; Lippert, B. *Angew. Chem., Int. Ed. Engl.* **1996**, *35*, 1228−1229. (b) McGowan, G.; Parsons, S.; Sadler, P. J. *Chem.—Eur. J.* **2005**, *11*, 4396−4404. (c) Saftić, D.; Žinić, B.; Višnjevac, A. *Tetrahedron* **2012**, *68*, 1062−1070. (d) Schimanski, A.; Freisinger, E.;

Erxleben, A.; Lippert, B. *Inorg. Chim. Acta* **1998**, *283*, 223−232. (e) Mandel, G. S.; Marsh, R. E. *Acta Crystallogr.* **1975**, *B31*, 2862−2868.
(22) Murata, T.; Nakamura, K.; Yamochi, H.; Saito, G. *Synth. Met.* **2009**, *159*, 2375−2377.
(23) Saito, G.; Ferraris, J. P. *Bull. Chem. Soc. Jpn.* **1980**, *53*, 2141−2145.
(24) Bondi, A. *J. Phys. Chem.* **1964**, *68*, 441−451.
(25) (a) Horiuchi, S.; Tokura, Y. *Nat. Mater.* **2008**, *7*, 357−366. (b) Horiuchi, S.; Tokunaga, Y.; Giovannetti, G.; Picozzi, S.; Itoh, H.; Shimano, R.; Kumai, R.; Tokura, Y. *Nature* **2010**, *463*, 789−793.
(26) Murata, T.; Saito, G. *Chem. Lett.* **2006**, *35*, 1342−1344.
(27) Destro, R.; Kistenmacher, T. J.; Marsh, R. E. *Acta Crystallogr.* **1974**, *B34*, 79−85.
(28) Corral, E.; Kooijman, H.; Spek, A. L.; Reedijk, J. *New J. Chem.* **2007**, *31*, 21−24.
(29) Bendeif, E.-E.; Dahaoui, S.; Benali-Cherif, N.; Lecomte, C. *Acta Crystallogr.* **2007**, *C63*, 448−458.
(30) Emge, T. J.; Maxfield, M.; Cowan, D. O.; Kistenmacher, T. J. *Mol. Cryst. Liq. Cryst.* **1981**, *65*, 161−178.
(31) O'Kane, S. A.; Clérac, R.; Zhao, H.; Ouyang, X.; Galán-Mascarós, J. R.; Heintz, R.; Dunbar, K. R. *J. Solid State Chem.* **2000**, *152*, 159−173.
(32) (a) Wiygul, F. M.; Ferraris, J. P.; Emge, T. J.; Kistenmacher, T. J. *Mol. Cryst. Liq. Cryst.* **1981**, *78*, 279−293. (b) Emge, T. J.; Wiygul, F. M.; Ferraris, J. P.; Kistenmacher, T. J. *Mol. Cryst. Liq. Cryst.* **1981**, *71*, 295−310.
(33) Wiygul, F. M.; Emge, T. J.; Ferraris, J. P.; Kistenmacher, T. J. *Mol. Cryst. Liq. Cryst.* **1981**, *71*, 303−314.
(34) Kistenmacher, T. J.; Emge, T. J.; Bloch, A. N.; Cowan, D. O. *Acta Crystallogr.* **1982**, *B38*, 1193−1199.
(35) Giorgi, T.; Grepioni, F.; Manet, I.; Mariani, P.; Masiero, S.; Mezzina, E.; Pieraccini, S.; Saturni, L.; Spada, G. P.; Gottarelli, G. *Chem.—Eur. J.* **2002**, *8*, 2143−2152.
(36) (a) Gellert, M.; Lipsett, M. N.; Davies, D. R. *Proc. Natl. Acad. Sci. U.S.A.* **1962**, *48*, 2013−2018. (b) Davis, J. T. *Angew. Chem., Int. Ed.* **2004**, *43*, 668−698.
(37) (a) Tang, H.; Cheng, F.-J.; Li, N.; Liu, Y.-C.; Chen, Z.-F. *Acta Crystallogr.* **2009**, *E65*, o2878. (b) Fletcher, S.; Shahani, V. M.; Lough, A. J.; Gunning, P. T. *Tetrahedron* **2010**, *66*, 4621−4632.
(38) Golobič, A.; Šarić, D.; Turel, I.; Serli, B. *Acta Chim. Slov.* **2008**, *55*, 973−977.
(39) (a) Low, J. N.; Tollin, P.; Young, D. W. *Acta Crystallogr.* **1986**, *C42*, 1045−1047. (b) Maixner, J.; Zachová, J. *Acta Crystallogr.* **1991**, *C47*, 2474−2476. (c) Wei, C. H. *Cryst. Struct. Commun.* **1977**, *6*, 525−529.
(40) (a) Purnell, L. G.; Hodgson, D. J. *J. Am. Chem. Soc.* **1976**, *98*, 4759−4763. (b) Terzis, A.; Mentzafos, D. *Inorg. Chem.* **1983**, *22*, 1140−1143.
(41) Sobell, H. M.; Tomita, K. *Acta Crystallogr.* **1964**, *17*, 126−131.
(42) (a) Kikuchi, H.; Nagasawa, H.; Ajiro, Y.; Asano, T.; Goto, T. *Physica B* **2000**, *284−288*, 1631−1632. (b) Helis, H. M.; Goodman, W. H.; Wilson, R. B.; Morgan, J. A.; Hodgson, D. J. *Inorg. Chem.* **1977**, *16*, 2412−2416. (c) Takahashi, N.; Okubo, S.; Ohta, H.; Sakurai, T.; Ishikawa, Y.; Fujisawa, M.; Kikuchi, H. *Appl. Magn. Reson.* **2011**, *40*, 481−487. (d) Khan, M. I.; Cevik, S.; Doedens, R. J. *Chem. Commun.* **2001**, 1930−1931.
(43) (a) Dagotto, E.; Rice, T. M. *Science* **1996**, *271*, 618−623. (b) Rovira, C. *Chem.—Eur. J.* **2000**, *6*, 1723−1729.
(44) Kim, K.; McComas, W. *Comb. Chem. High Throughput Screen* **2000**, *3*, 125−129.
(45) Ciapetti, P.; Taddei, M. *Tetrahedron* **1998**, *54*, 11305−11310.
(46) Lu, W.; Sengupta, S.; Petersen, J. L.; Akhmedov, N. G.; Shi, X. *J. Org. Chem.* **2007**, *72*, 5012−5015.
(47) Sheldrick, G. M. *Program for the Solution of Crystal Structures*; University of Göttingen: Göttingen, Germany, 1997.
(48) Burla, M. C.; Caliandro, R.; Camalli, M.; Carrozzini, B.; Cascarano, G. L.; De Caro, L.; Giacovazzo, C.; Polidori, G.; Spagna, R. *J. Appl. Crystallogr.* **2005**, *38*, 381−388.
(49) Sheldrick, G. M. *Program for the Refinement of Crystal Structures*; University of Göttingen: Göttingen, Germany, 1997.